CHAPTER ONE

INTRODUCTION

1.1 BACKGROUND OF THE STUDY

Tribology is derived from the Greek word “tribos”, which means “to rub”. Nanotribology is the study of friction, lubrication and wear at atomistic length and time scales. This is a really challenging field and requires much inter-disciplinary co-operation (Carpick and Salmeron, 1997). The invention of atomic force microscope (AFM) removed many barriers placed by scanning tunneling microscope in nanotribology investigations. Sample conductivity was no longer a requirement, hence, new classes of important materials like insulators and large band-gap semiconductors were brought into the realm of atomic-scale scanning probe measurements (Krim, 2012). Extracting information about nanotribological properties of materials has numerous practical importance. Reducing energetic losses due to friction which will help a car engine to work efficiently, utilizing friction as an operating mechanism in car brakes, reducing material losses due to wear (e.g. longer-lasting tires) and optimizing lubricants (e.g. increasing the efficiency and life time of engine parts) are important issues for a wide range of industrial and societal applications. In fact, it is estimated that a substantial portion of a nation’s gross domestic product is dispensed on energetic or mechanical losses due to friction

and wear and a significant portion of this could realistically be recovered by improvements achieved through research (Carpick and Salmeron, 1997). With the invention of small devices, triggered in part by the tremendous development of silicon micro fabrication techniques, novel problems appear that require knowledge at the nanometer scale. For example, the whole technology of information storage as shown by the case of computer hard disks with coatings and lubricants that protects the stored information, with dimensions that are measured in nanometers. Micrometer-sized actuators, sensors, and motors are other examples of novel technology requiring such knowledge for performance optimization.

Despite practical successes recorded so far, yet friction is one of the most common but least understood physical phenomena (Honma and Nose, 2007). The major reason for this lack of understanding is that probing the atomic processes taking place at a buried interface is an inherently difficult task. The main conclusion of the earlier observations, as most high school physics students learn is that friction between a pair of surfaces is proportional to load (normal force). Furthermore, friction is evidently independent of apparent area of contact and only weakly dependent on the relative sliding velocity. This linear dependence of friction on load is a result of complex phenomena at the interface, particularly multiple asperity contact, adhesion–induced deformation

and plowing of the surfaces by wear particles during sliding. While these observations are important, they could not explain the behaviour at atomic scale and cannot be used for predictive analysis (Jang *et al.*, 2007).

At the fundamental level, friction, wear and adhesion need to be understood in terms of chemical bonding and of the elementary processes that are involved in the excitation and dissipation of energy modes. One of such processes is due to coupling to the substrate and tip electron density that causes a drag force, similar to that causing an increase in electrical resistance by the presence of surfaces in thin films. Another is the excitation of surface phonon modes in atomic stick-slip events (Joly-Pottuz *et a*l., 2007).

Delocalization of the excited phonons by coupling to other phonon modes through anharmonic effects and transport of the energy away from the excited volume leads to efficient energy dissipation. At high applied forces, wear processes leading to rupture of many atomic bonds, displacement and creation of dislocations and debris particles are important and are part of the wide topic of plastic deformation of materials.

The next level of complexity in understanding tribology includes the questions such as the nature of the relative motion between the two contacting bodies. Is the motion continuous (smooth sliding) or discontinuous (stick-slip)? How does friction depend upon the actual area of contact between a pair of

materials? Are friction and adhesion related? What is the behaviour of lubricant molecules at an interface? How are they compressed and displaced during loading and shear? How does their behaviour depend on their molecular structure and chemical identity? The relatively recent development of techniques that probe the properties of interfaces with either atomic-scale spatial or temporal resolution has generated great interest because these fundamental questions are beginning to be addressed. This excitement stems not only from the development of atomic force microscope (AFM), but also from the recent advances with other instruments such as the quartz-crystal microbalance (QCM) and the extension of the surface force apparatus (SFA) to measure frictional forces (Carpick and Salmeron ,1997).

Furthermore, advances in computational power and theoretical techniques are now making sophisticated atomistic models and simulations feasible. By using these techniques to address the questions outlined above, the knowledge gained could be used in combination with the highly developed fields of chemical engineering, material processes and synthesis and engineering design to produce machines and devices with optimal tribological performance (La Rosa *et al.*, 2005).

The typical approach to reducing friction is to optimize the properties of the surfaces that come into contact with each other. The idea is to make friction

low by the appropriate choice of chemical composition, crystal structure, surface roughness, electrostatic interactions and other properties. Considerable progress has been made over the past decade with special coatings such as the family of diamond-like carbon films (Frenken, 2006). More delicate but perhaps less practical ways to reach ultralow friction involves either an extreme reduction of the contact pressure or a cancellation of lateral forces. This later goal can be achieved by making use of the non-periodicity of quasicrystals or by introducing a deliberate lattice mismatch between the two sliding crystal surfaces (a mechanism referred to as superlubricity). What these techniques all have in common is that they change the energy landscape of the interaction between the surfaces at the atomic scale.

Recently, two new methods have been demonstrated that enable researchers to vary friction continuously by use of an easily adjusted external control parameter - increasing the friction in one case and decreasing it in the other. Both experiments were performed under ultra high vacuum with atomic force microscopes (AFMs) that were operated as lateral or friction force microscopes (Carpick and Salmeron, 1997). In a traditional AFM, an ultra-sharp tip on a cantilever is scanned over a surface, and the forces between the surface and the tip cause the cantilever to bend in the vertical direction (that is at right angles to the surface). By measuring the deflection of the cantilever, it

is possible to produce an image of the surface with atomic resolution. Also, by monitoring how the cantilever twists, the amount of friction can be determined. The approach described at the Lawrence Berkeley national laboratory in California and the Ames laboratory in Iowa involves a controversial contribution to the friction force, namely electronic friction. The extent to which electronic effects, such as the generation of pairs of electrons and holes determine the energy dissipation rate of a sliding contact has been a long-standing matter of debate, and only a few experiments have managed to probe these effects. It was convincingly demonstrated that electronic effects are significant by measuring the friction force between the tip of a friction force microscope (FFM) and a piece of n-type silicon that contains strips of p-type silicon. The p-type strips were written by implanting boron into the surface. To make sure that structural and chemical details of the surface were not responsible for spatial variations of the lateral force, the entire surface was coated with a thin oxide layer. Under this condition, two parameters could be adjusted independently; the normal force with which the tip was pressed against the surface and an electrostatic voltage that could be applied between the silicon and the tip (Frenken, 2006; Lee and Kui, 1994).

The basic paradigm of nanotribological research is that the frictional behaviour of a single asperity contact needs to be clarified in order to

understand friction better in complex macroscopic systems. Naturally, this makes the friction force microscope a tool of choice for nanotribology research (Hölscher *et al.*, 2008).

In most third-world countries especially in African continent, AFM and FFM are hard to come by. This makes it extremely difficult for scientists in these countries to carry out experimental research in nanotribology. However, it is known that the stick-slip phenomena observed in these experiments with FFM and AFM can be understood in the framework of the well established Prandtt-Tomlinson (PT) model (Liu and Bhushan , 2004) which is sometimes also referred to as independent oscillator model. This research work therefore tends to establish functional theoretical models which can be used to study various nanotribological parameters with results that will compare favourably with experimental results.

1.2 STATEMENT OF PROBLEM

Nanotribology is a very important aspect of nanotechnology. Information about nanotribological properties of materials is required in many areas especially in miniaturized systems. Presently, the well known Tomlinson model which has addressed tribology is a classical model and cannot function effectively at nano-level. Hence, the need to develop quantum Tomlinson models which can be used to study nanotribology of semiconductors including binary compounds. These

models will also help to complement the existing equipment for nanotribology research like atomic force microscope and friction force microscope.

1.3 AIM AND OBJECTIVES

The aim of this research work is to develop functional quantum Tomlinson models which can be used to study nanotribology of semiconductor surfaces.

The objectives of the study include:

1. To develop quantum Tomlinson models which can be used to study three different parameters of nanotribology of semiconductors.
2. To use these models to study the following parameters of nanotribology of semiconductor surfaces:

a. Temperature dependence of nanotribology

b. Velocity dependence of nanotribology.

c. Normal load dependence of nanotribology.

3. To ensure that these models are sensitive enough to predict experimental results at nano-scale.
4. To use these models to predict experimental results for seven different semiconductors.
5. To provide a theoretical approach as an alternative to experimental research.

1.4 SCOPE OF STUDY

This study concentrates on the following:

1. Using Bond-orbital model and Tomlinson model to develop jump energy quantum models for high and low ionic energy gaps.
2. Combination of Tomlinson model and Sang's equation to develop temperature model.
3. Transformation and modification of the temperature model to develop low and high velocity models.
4. Further transformation and modification of the temperature model to develop normal load model.
5. To use jump energy quantum models to calculate the energy barrier ΔE for all the semiconductors under study.
6. Use of temperature model to predict results for temperature dependence of nanotribology for all the six semiconductors.
7. To use low and high velocity models to predict results for velocity dependence of nanotribology for the six semiconductors.
8. Using the normal load model to predict results for normal load dependence of nanotribology for all the semiconductors under study.

CHAPTER TWO

LITERATURE REVIEW

2.1 Semiconductors

A material which has only completely full and completely empty bands is called an insulator. If the distance between the upper edge of the highest filled band (valence band) and the lower edge of the lowest empty band (conduction band) is not too large (e.g. approx. 1 eV), then the finite width of the region over which the Fermi distribution changes rapidly has observable consequences at moderate and high temperatures. A small fraction of the states in the vicinity of the upper edge of the valence band is unoccupied and the corresponding electrons are found in the conduction band. Both these thermally excited elections and holes that leave the conduction band can carry current. Materials that possess these characteristics are called semiconductors (Ibach and Luth, 2004). There are only three semiconducting elements, namely, the group IV elements [silicon, germanium and gray tin] of the periodic table (Animalu, 1977). Due to a mixing of s and p wavefunctions, tetrahedral bonding orbital (sp^3) are formed which for a bonding distance near equilibrium leads to a splitting into bonding and antibonding orbitals. The bonding orbitals constitute the valence band and the antibonding orbitals the conduction band. Since the

formation of sp^3 hybrids is obviously important in the chemical bonding of Si and Ge we might expect semiconducting properties in other materials with tetrahedral crystal structure i.e with sp^3 hybridization. Based on this, we identify another important class of the III-V semiconductors, which are compounds comprising elements from the third and fifth groups of the periodic table. Examples are: InSb, InAs, InP, GaP, GaAs, GaSb and AlSb. In these compound crystals, the bonding is mixed ionic and covalent. The mixed bonding can be imagined as a superposition of two extreme cases, the ionic, in which the election transfer from Ga to As gives an ionic structure Ga^+ As^- and the covalent in which electron displacement from As to Ga leaves both Ga and As with four electrons in the outer shell and thereby allow the formation of sp^3 hybrids just as in Si and Ge. This later covalent structure is dominant. In contrast to the elemental semiconductors, the most important representatives of the III- V semiconductors possess a so-called direct band gap, i.e. the valence band maximum and conduction band minimum both lie at the same k-point . There are three distinct valence bands with a qualitatively similar form at Γ to those of the tetrahedral elemental semi-conductors. Although GaP and AlSb are III-V semiconductors, they have indirect band gaps i.e. similar to Si and Ge (Ibach and Luth, 2004).

Similar arguments to those presented for the case of III-V semiconductors leads to an understanding of the II-VI semiconductors such as ZnO, ZnS, CdS, and CdTe. These compounds have direct band gaps. In these compounds there is also a mixed ionic-covalent bonding, but with a larger ionic component than for the III-V semiconductors . The crystal structure is either that of the III-V semiconductors (ZnS) or that of Quartzite. In both cases the local structure is tetrahedral, which can again be attributed to the sp^3 hybridization of the bonding partners (Ibach and Luth, 2004).

2.2 NANOTRIBOLOGY

Nanotribology can be defined as the investigations of interfacial processes on scales ranging in the molecular and atomic scales occurring during adhesion, friction, scratching, wear, nanoindentation and thin-film lubrication at sliding surfaces (Chandross *et al*., 2004; Chang and chang, 2007; Williams *et al.*, 2008) . With improvements in properties with decreasing size observed in the field of nanotechnology, nanotribology is today one of the most important technologies.

Friction is an old subject of research. Two different types of friction are commonly defined. Static friction, F_s, is the lateral force that must be applied to initiate sliding of one object over another, while kinetic friction, $F_{k,}$ is the lateral force that must be applied to maintain sliding. At macroscopic level, both forces usually obey Amonton's laws, which states that friction is proportional

to the load pushing the surfaces together and is independent of area (Martin, 2004; De Boer *et al*., 2010). Macroscopic experiments systematically performed by the school of Bowden and Tabor have revealed that macroscopic friction can be related to the collective action of small asperities. During the last 15years, experiments performed with the Atomic force microscope (AFM) gave new insight into the physics of single asperities sliding over surfaces. This development together with complementary experiments by means of surface force apparatus (SFA) and quartz-crystal microbalance established the new field of nanotribology and at the same time, increasing computing time allowed for the simulation of the processes in sliding contacts consisting of several hundred atoms (Gnecco *et al.,* 2010). It became clear that atomic processes cannot be neglected in the interpretation of nanotribology experiments. Experiments on even well-defined surfaces directly revealed atomic structures in friction forces. Over the years, some functional equipment have been developed to study this all important field of nanotechnology. These include: surface force apparatus (SFA), scanning tunneling microscope (STM), atomic force microscope (AFM), and friction force microscope (FFM). SFA was developed in the 1960s (Bhushan and Marti, 2010) and has been commonly used to study the static and dynamic properties of molecularly thin films sandwiched between two molecularly smooth surfaces. STM was developed in 1981(Bhushan, 2010) and has since then been used to image clean conducting

surfaces and lubricant molecules. The STM has a resolution in the atomic level. AFM was developed in 1985 (Carpick and Salmeron , 1997) and its common uses are:

- Measuring ultra – small forces between probe tip and the surface.
- Topographical measurements on the nanoscale.
- Adhesion force measurements.
- Electrostatic force measurements.
- Investigating scratching, wear and indentation.
- Detection of transfer of material.
- Boundary lubrication.
- Fabrication and machining.

The friction force microscope (FFM) is a modified form of the AFM and gives the atomic and micro scale studies of friction and lubrication. The FFM also known as lateral force microscope (LFM) uses a sharp diamond tip mounted on a stiff cantilever beam. However, AFM is the most commonly used equipment for nanotribology research (Carpick and Salmeron, 1997).

2.3 OPERATION MODES OF NANOTRIBOLOGY INSTRUMENTS: FRICTION FORCE MICROSCOPY IN ULTRA HIGH VACUUM.

The friction force microscope exploits the interaction of a sharp tip sliding on a surface to quantify dissipative processes down to the atomic scale. The relative motion of the tip and surface is realized by a scanner formed by piezo-

electric elements which moves the surface sample perpendicularly to the tip with a certain periodicity. The scanner can also be extended or retracted in order to vary the normal force F_N which is applied on the surface. This force is responsible for the deflection of the cantilever that supports the tip. If the normal force F_N increases while scanning due to the local slope of the surface, the scanner is retracted by a feedback loop. On the other hand if F_N decreases, the surface is brought closer to the tip by extending the scanner. In this way, the surface topography can be determined line by line from the vertical displacement of the scanner. An accurate control of such vertical movement is made possible by a light beam which is reflected from the rear of the lever into a photodetector. When the bending of the cantilever changes, the light spot on the detector moves up or down and causes a variation of the photocurrent that corresponds to the normal force F_N to be controlled. Usually the relative sliding of tip and surface is also accompanied by friction. A lateral force, F_L, in the opposite direction of the scan velocity, V, hinders the motion of the tip (Anczykowski, 2004; Gnecco *et al.*, 2010). This force provokes the torsion of the cantilever and it can be observed with the topography if the photodetector can reveal not only the normal deflection but also the lateral movements of the lever while scanning. In practice this is realized by four-quadrants photodetectors as shown in Fig. 2.1. It should be noted that friction forces also cause the lateral bending of the cantilever, but this effect is negligible if

the thickness of the lever is much less than the width. The FFM was first used in 1987 to reveal friction with atomic features just one year after the atomic force microscope was introduced. (Mate, *et al*., 1987).

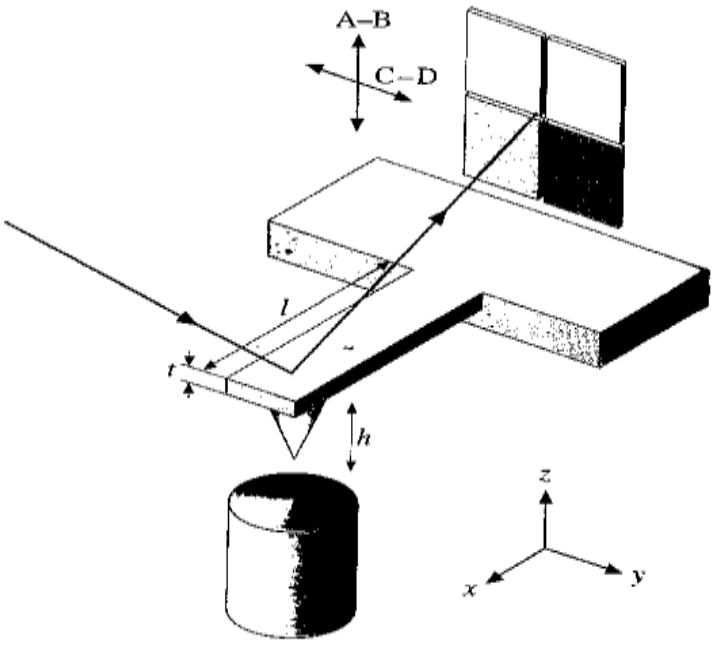

Fig. 2.1: Schematic diagram of a beam-deflection friction force microscope (Gnecco et al., 2010)

In an experiment, a tungsten wire and a slightly different technique was used to detect lateral forces (non-fiber interferometry). The optical beam deflection was introduced later (Gnecco *et al.*, 2010). Other methods to measure the forces between tip and surface are given by capacitance detection, dual fiber interferometry and piezolevers. In the first method, two plates close to the cantilever reveal capacitance while scanning. The second technique uses two

optical fibers to detect the cantilever deflection along two orthogonal directions angled 45^0 with respect to the surface normal. Finally in the third method, cantilevers with two wheatstone bridges at their bases reveal normal and lateral forces which are respectively proportional to the sum and the difference of both bridge signals.

A typical atomic force microscope (AFM) for ultra-high vacuum application is shown in Fig. 2.2.

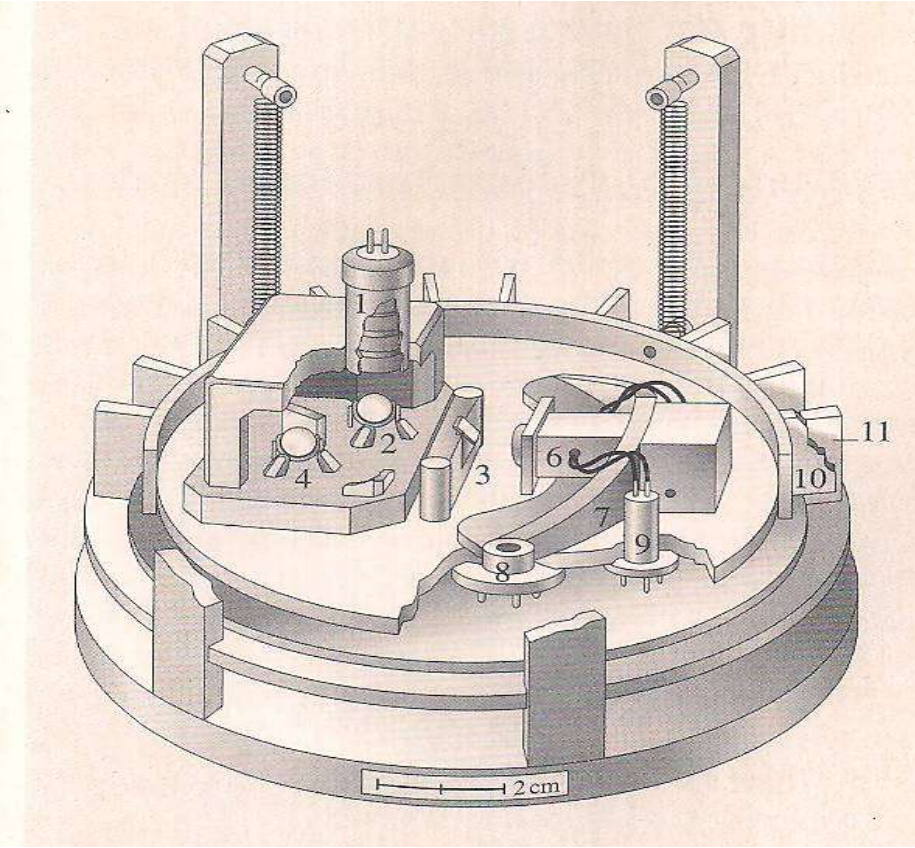

Fig. 2.2. Schematic view of atomic force microscope (Liu and Bhushan, 2004).

The housing (1) contains the light source and a set of lenses that focus the light onto the cantilever. Alternatively, the light can be guided via an optical fiber into the vacuum. By using light emitting diodes with low coherency, disturbing interference effects often found in instruments equipped with lasers as light source are avoided. A plane mirror fixed on the spherical rotor of a first stepping motor (2) can be rotated around vertical and horizontal axes to guide the light beam onto the rear of the cantilever mounted on a removable carrier plate (3). The light is reflected off the cantilever towards a second motorized mirror (4) that guides the beam to the center of the quadrant photodiode (5), where the light is then converted into four photo-currents. Four pre-amplifiers in close vicinity to the photodiode allow low-noise measurements with 3 MHz bandwidth (Gnecco *et al*., 2010).

The two motors with spherical rotors, used to realign the light path after exchange of the cantilever work as inertial stepping motors. The sphere is resting on three piezoelectric legs that can be moved by a small amount tangentially to the sphere. Each step of the motor consists of a slow forward motion of two legs followed by an abrupt jump backwards. During the slow forward motion the sphere follows the legs due to friction, whereas it cannot follow the sudden jump due to its inertia. A series of such tiny steps rotates the sphere macroscopically. The sample also on an exchangeable carrier plate is mounted on the end of a tube scanner (6), which can move the sample in three dimensions over several micrometers. The

whole scanning head (7) is the slider of a third inertial stepping motor for course positioning of the sample. It rests with its flat and polished bottom on three supports. Two of them are symmetrically placed piezoelectric legs (8) whereas the third central support is passive. The slider (7) can be translated in two dimensions and rotated about a vertical axis by several millimeters (rotation is achieved by antiparallel operation of the two legs). The slider is held down by two magnets close to the active supports and its travel is limited by two fixed posts (9) that also serve as cable attachments. The whole platform is suspended by four springs. A ring of radial copper lamellae (10), floating between a ring of permanent magnets (11) on the base flange, acts as efficient eddy current damping.

In an AFM experiment, a small sharp tip (with a radius typically between 10-100nm) is attached to the end of a compliant cantilever. The tip is brought into close proximity with a sample. Surface forces acting between the AFM tip and the sample will result in deflections of the cantilever (Batteas, 2004;
Gnecco *et al*., 2010). The cantilever bends vertically (i.e towards or away from the sample) in response to attractive and/or repulsive forces acting on the tip. When the tip is in contact with the sample, the deflection of the cantilever from its equilibrium position is proportional to the normal load applied to the tip by the cantilever. Lateral forces result in a twisting of the cantilever from its equilibrium position. These measurements can be performed in a variety of environments:

ambient air, controlled atmosphere, liquids or ultra high vacuum. Atomic force microscope is certainly the most versatile tool for nanotribology research in terms of operating environment (Carpick and Salmeron, 1997). There are different force regimes in which forces can be measured with AFM. Fig. 2.3 below shows the normal force typically experienced by the tip as it is brought towards a sample surface.

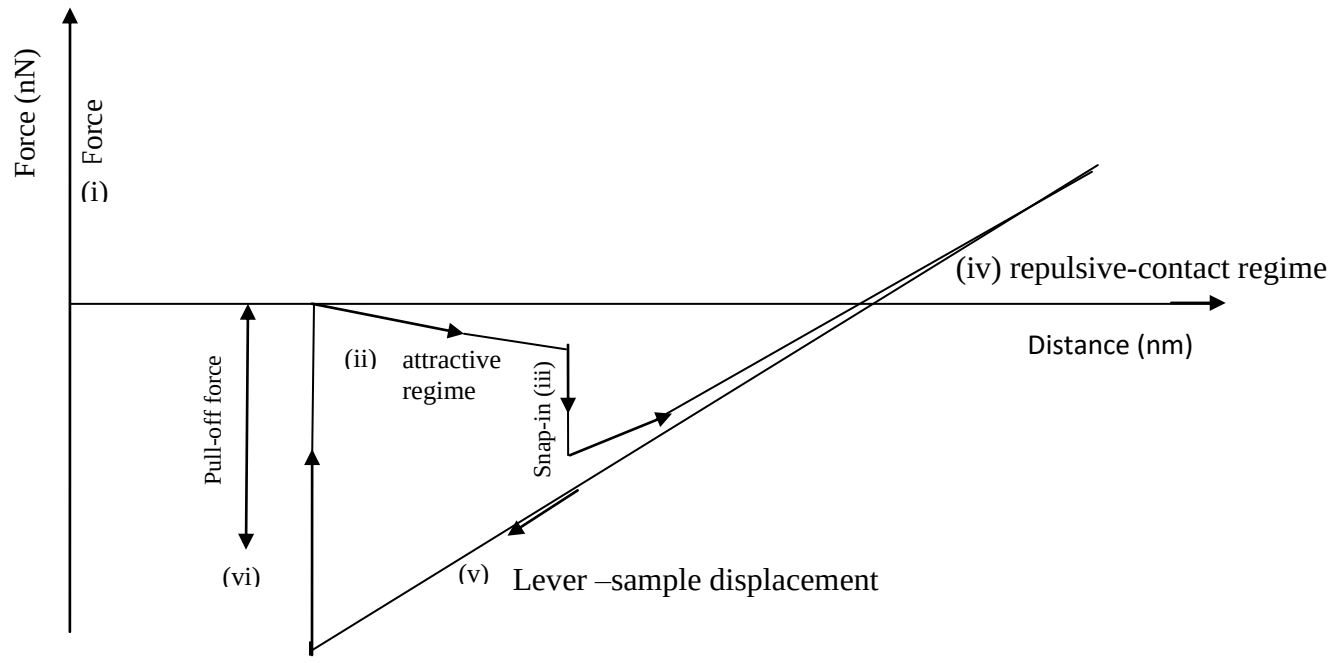

Fig. 2.3. Typical force experienced by the AFM tip (Carpick and Salmeron, 1997)

"Force-distance" curve displays the vertical cantilever bending vs. lever sample displacement. This displacement is measured between the sample and the rigidly rear end of the cantilever (as opposed to the front end with

the tip which will bend in response to interaction forces).

(i) The lever and sample are initially far apart and no forces act.

(ii) As the lever is brought close to the sample, the tip senses attractive forces which cause the end of the lever to bend downwards, thus signifying a negative (attractive) force.

(iii) The attractive force gradient exceeds the spring constant of the lever at this point, and this instability causes the tip to snap into contact with the sample.

(iv) The lever sample displacement can continue to be reduced. Since this tip is in repulsive contact with the sample, the front end of the lever is pushed further and further upward. The force corresponds to the externally applied load.

(v) The motion is reversed. Adhesion between the tip and sample maintains the contact although there is now a negative (tensile) load.

(vi) Finally the (tensile) load overcomes the adhesion or a pull-off force and the tip snaps out of contact with the sample, (Carpick and Salmeron, 1997).

Two force regimes can be distinguished, the "attractive regime" where interaction forces (Van der Waals, electrostatic, etc) attract the tip to the sample but actual mechanical contact does not occur, and then the "repulsive" or "contact regime" where the outer electronic configuration of tip and sample atoms provide electrostatic and Pauli repulsive forces (Mann, 2004). On approach these two regimes are separated by a snap-in instability which occurs when the attractive force gradient exceeds the spring constant of the cantilever. Interfacial surface forces between the tip and sample lead to adhesion during contact. The lateral twisting of the cantilever (F_L) can be measured simultaneously with topography and often features that are not necessarily topographically distinct can show contrast in the lateral force signal due to different friction characteristics. This suggests that friction imaging can have some degree of material or chemical sensitivity. Lateral force images often display atomic scale stick-slip behavior with the periodicity of the atomic lattice of the sample (Carpick and Salmeron, 1997).

For normal force (F_N) measurement, a feedback circuit is enabled to vary the relative vertical displacement (F_N) as the tip is rastered across the sample. In this case, the control signal kept constant is cantilever deflection. Such constant force images can be obtained in either the attractive or repulsive regimes. It should be pointed out that when the tip is in mechanical contact with a given sample, simple elastic contact mechanics show that for typical tip radii, loads and elastic constants,

the contact is not just a single atom. For example a 20nm radius silicon nitride tip (sharp by AFM standards) exerting a 1nN load (relatively low by AFM standards) on a mica sample produces a contact area involving nearly 15 mica unit cells. Contact mode atomic force microscope therefore does not possess single atom resolution as with STM and so point defects are not imaged and the nature of observed atomic corrugations is complicated. This finite contact area is the essential limit on the lateral resolution of features and result in effects such as finite atomic step widths (Carpick and Salmeron, 1997).

Generally, AFM relies on a scanning technique to produce very high resolution 3-dimension images of sample surfaces. It measures ultra small forces (less than 1nN) present between the AFM tip surface mounted on a flexible cantilever beam and a sample surface, (Bhushan and Marti, 2010). These small forces are determined by measuring the motion of a very flexible cantilever beam with an ultra small mass. The deflection can be measured to within 0.02nm, so for a typical cantilever spring constant of 1.0N/m, a force as low as 0.2nN can be detected. To put these numbers in a clearer perspective, we note that individual atoms and human hair are typically a fraction of nanometer and about 75μm in diameter, respectively. A drop of water and an eyelash have masses of about 10μN and 100nN respectively. In the operation of a high resolution AFM, the sample is generally scanned, rather than the tip because any cantilever movement would add

vibrations. However, in large sample measurements, the tip is scanned while the sample is stationary. To obtain atomic resolution with AFM, the spring constant of the cantilever should be weaker than the equivalent spring between atoms. A cantilever beam with a spring constant of about 1N/m or lower is desirable. For high lateral resolution, tips should be as sharp as possible (Bhushan, 2010).

A modification of AFM providing a sensor to measure the lateral force led to the development of friction force microscope (FFM), or the lateral force microscope (LFM) designed for atomic-scale and micro scale studies of friction and lubrication. This instrument measures lateral or friction forces (in the plane of sample surface and in the scanning direction) by using a standard or a sharp diamond tip mounted on a stiff cantilever beam. AFM is also used in investigations of scratching and wear, indentation, fabrication/machining and surface roughness, including atomic-scale imaging. Adhesion, wear, friction and boundary lubrication at the surface between two solids with and without liquid films were studied using AFM and FFM (Carpick and Salmeron, 1997; Bhushan, 2010).

In a small sample AFM, the sample general not larger than 10mm x 10mm, is mounted on a piezoelectric tube (PZT) scanner that consists of a separate electrodes to scan precisely the sample in x-y plane in a raster pattern and move it in the vertical (Z) direction. A sharp tip at the free end of a flexible cantilever is brought in contact with the sample. Normal and frictional forces being applied at

the tip-sample interface are measured using a laser beam deflection technique. A laser beam from a diode laser is directed by a prism onto the back of a cantilever near its free end, which is tilted downwards at about 10^{o} with respect to the horizontal plane. The reflected beam from the vertex of the cantilever is directed through a mirror onto a quad photo-detector. The differential signal from the top and bottom photo-diodes provides the AFM signal, which is a sensitive measure of the cantilever vertical deflection (Hafner, 2004). Topographic features of the sample causes the tip to deflect in the vertical direction as the sample is scanned under the tip. This tip deflection will change the direction of the reflected laser beam, changing the intensity difference between the top and bottom sets of photodetectors (AFM signal). In the AFM operating mode, called the height mode, for topographic imaging, or for any other operation in which the applied normal force is to be kept constant, a feedback circuit is used to modulate the voltage applied to the PZT scanner to adjust the height of the PZT, so that the cantilever vertical deflection (given by the intensity difference between the top and bottom detectors) will remain constant during scanning (Bhushan, 2010). The PZT height variation is thus a direct measure of the surface roughness of the sample. In a large sample AFM, both force sensors using optical deflection method and scanning unit are mounted on the microscope head. Because of vibrations added by cantilever movement, lateral resolution of this design is somewhat poorer than the small

sample AFM design in which the sample is scanned instead of cantilever beam. The advantage of the large samples AFM is that large samples can readily be measured. AFMs can also be used for topography measurements in the so-called tapping mode (intermittent contact mode). In the tapping mode during scanning over the surface, the cantilever/tip assembly is sinusoidally vibrated by a piezo mounted above it, and the oscillating tip slightly taps the surface at the resonant frequency of the cantilever oscillating in vertical direction with a feedback loop keeping the average normal force constant. The oscillating amplitude is kept large enough so that the tip does not get stuck to the sample because of adhesive attractions. The tapping movement is used in topography measurements to minimize the effects of friction and other lateral forces and to measure topography of soft surfaces (Gnecco *et al.*, 2010).

For measurement of friction force applied at the tip surface during sliding, left-hand and right-hand sets of quadrants of the photodetector are used. In the so-called friction mode, the sample is scanned back and forth in a direction orthogonal to the long axis of the cantilever beam. A friction force between the sample and the tip will produce a twisting of cantilever. As a result, the laser beam will be reflected out of the plane defined by the incident beam and the beam reflected vertically from an untwisted cantilever. This produces an intensity difference of the laser beam received in the left-hand and right-hand sets of quadrants of the photo-

detector (Carpick and Salmeron, 1997). The intensity difference between the two sets of detectors (FFM signal) is directly related to the degree of twisting and hence to the magnitude of the friction force. One problem associated with this method is that any misalignment between the laser beam and the photodetector axis would introduce error in the measurement. However, by following the procedures in which the average FFM signal for the sample scanned in two opposite directions is subtracted from the friction profiles of each of the two scans, the misalignment effect is removed. This method provides three dimensional maps of friction force. The coefficient of friction can be obtained from the slope of friction force data measured as a function of normal loads typically ranging from 10-150nN. This approach eliminates any contribution due to the adhesive forces (Bhushan, 2010). For calculation of coefficient of friction based on a single point measurement, friction force should be divided by the sum of applied normal load and intrinsic adhesive force. For single asperity contact, the coefficient of friction is not independent of load. Generally, friction measurements are normally carried out in the load range of 10-150nN.

2.4 **PHONONIC FRICTION**

Tomlinson published an early model in 1929 of how friction might in fact originate at the microscale (Tomlinson, 1929). In this model, when two surfaces slip across each other, wear-free friction can occur due to the vibrations of the

atomic lattices. The atoms close to one surface vibrate when the atoms in the opposite surface slip across them. These vibrations are called phonons, or sound waves. The phonons dissipate energy as heat and this microscopic process is manifested as friction. Motivated by Tomlinson's model, attempts were made at Cambridge University in the 1960's to detect evidence for the phononic contributions to friction but there was no success. Decades later, the concept of phononic friction was independently revisited (Sokoloff *et al.*, 1978; Sacco and Sokoloff ,1978; Mate *et al*.,1987). Following these efforts, models similar to the original work of Tomlinson were rederived. Subsequently lateral force microscope was developed for studies of atomic scale friction in an effort to observe phononic mechanism for friction (Mate *et al.*, 1987). To date, the technique has unearthed no direct evidence for phononic mechanisms of friction. It has nonetheless proven to be a revolutionary new probe for studies of atomic scale friction in particular, and nano-scale science in general.

In 1991, quartz crystal microbalance (QCM) measurements of the friction of krypton monolayers sliding on Au (111) was reported (Krim *et al*., 1991). It was found that solid krypton monolayers sliding on Au (111) had five times longer slip times (lower friction) than liquid monolayers of krypton. In 1994, these interesting results were modeled (Cieplak *et al*.,1994). Using standard molecular dynamics algorithms, experimental results of Krim and colleagues were reproduced .

The simulations included only one source of friction, phononic friction. Given the close match between the simulations and the QCM experiments, it was concluded that phononic friction was the major source of friction for the krypton on Au (111) system. The combined QCM and numerical results provided the first definitive evidence for the existence of a phononic mechanism of friction (Cieplak *et al*., 1994; Krim, 2012).

2.5 ELECTRONIC FRICTION.

In addition to phononic friction, there is another type of dissipation mechanism, electronic that takes place in electrically conductive materials. In both electronic and phononic friction, kinetic energy associated with the sliding motion at an interface is transformed to heat. The heat is associated with temperature increases in both materials in sliding contact and is reflected in the phonon populations therein (Fujita *et al.,* 1998). Phononic dissipative mechanisms involve direct transfer of energy into the phonon populations, in contrast to electronic mechanisms which involve energy transfer into the conduction electrons before transfer into the phonon populations. In one proposed mechanism for electronic friction, the presence of another surface or an adsorbate and the sliding across the metal substrate causes excitation of the conduction electrons near the surface. The excitations generate electron-hole pairs. Electron-hole pairs in metals (in contrast to semiconductors) have very brief life times. When these electron-hole pairs relax,

the excess energy is dissipated as heat, and the temperature concomitantly rises. The mechanism is quite distinct from the forces associated with static charge buildup on insulating materials.

Persson (1991) has suggested that the electronic component of friction μ_{eh} is related to the surface resistivity of an adsorbate-substrate system by

$$\mu_{eh} = \frac{n^2 e^2 d \Delta\rho}{m n_a} \qquad (2.1)$$

'n' is number of conduction electrons per unit volume, 'e' is the electron charge, 'd' is the thickness of the metal film, $\Delta\rho$ is the adsorbate-induced increase in film resistivity, 'm' is the adsorbate mass and 'n_a is the number of adsorbates per unit area in direct contact with the substrate. This is derived for a viscous friction law of the form

$$F_{fric} = m\mu_{eh} V \qquad (2.2)$$

Where F_{fric} is the friction force and V is the sliding speed. Definitive proof of electronic contributions to friction is of great interest, since to date the vast majority of fundamental theoretical treatments of friction have considered phonon contributions only. Equation (2.1) was used to infer friction coefficients for a range of adsorbates and it was found that the slip times are in the range 10^{-9} – 10^{-12} seconds. The values compared favourably with slip times measured by means of quartz- crystal microbalance (QCM), which probes the total friction (Smith *et a*l., 1996). In an attempt to quantify the relative contributions of electronic friction and

phononic friction, the electronic friction calculated from electrical resistivity measurements was compared with the total friction taken from QCM measurements for xenon on Ag (111) at 77K (Dayo and Krim, 1998). It was observed that the resistivity of the Ag (111) film increases monotonically with the adsorption of the Xe, up to coverages of one monolayer. Above one monolayer the resistivity increases only very slightly. However the friction force per unit area required to slide the two-layer thick Xe film was 27% greater than that required to slide the monolayer film (Daly and Krim, 1996). Using equation (2.1), the electronic contribution to friction was calculated and compared to the total friction obtained from the QCM. It was found that the electronic contribution was at most 30% of the total for Xe/Ag (111) (Daly and Krim, 996). There have been several efforts to model the sliding of Xe/Ag (111). In some of these efforts, the models indicate that phononic friction dominates. It was reported that the increased number of possible vibrational modes that dissipate energy is greater for a bilayer than a monolayer and that this is the cause of the increase in friction (Tomassone *et al*., 1997). In models of the Xe/Ag (111) system by Persson and Nitzan, however, the increase in friction from the monolayer to the bilayer was reported to be caused by an increase in the electronic friction. They reported that the second layer pushes the Xenon closer to the silver surface, thus increasing the Van der Waals contribution to the electronic friction.

More direct evidence supporting the importance of the electronic contributions to friction was later published (Dayo *et al*., 1998). The sliding of thin nitrogen films adsorbed on lead surfaces was studied by means of QCM and the friction coefficient was observed to drop by almost half when the substrate became super conducting. The result drew much attention and sparked criticism as well, (Novotny and Velicky, 1999). A somewhat similar experiment found no slippage whatsoever of a nitrogen film at low temperature and thus no changes in the friction across the super conducting transition (Renner *et al*., 1999). Subsequently, it became clearer that the effect is observable only on substrates of extremely high purity. The experiment remains theoretically puzzling.

Tribologists are not the only research community to have pondered over energy dissipation mechanisms at moving interfaces. An entirely distinct surface science community emerged in later 1980's and the members studied both phononic and electronic contributions to energy dissipation within the context of small vibrational motions of atoms on surfaces (Anna *et al*., 1997;

Ruffel *et al.*, 2007). Whenever atoms or molecules adsorb on surfaces, new vibrational modes will emerge which are not present in either an isolated surface or the adsorbate alone. The modes which appear include both internal (stretching or torsional vibrations within a molecule) and "external" modes whereby the entire molecule or atom moves as a whole with respect to the surface. These phonon

modes for adsorbate-substrate systems can be measured by Helium Atom Scattering (HAS) and related spectroscopes (Toennies, 1993). They can also measure the line width (the life time or damping) of adsorbate vibrations, which is indicative of the rate at which the energy of the phonon mode is dissipated into heat. The line width of the adsorbate vibration has been shown to be linearly proportional to the friction coefficient (Persson, 1991). Frustrated translational modes both parallel and perpendicular to the substrate have been measured. Perpendicular modes (S-modes or FT_z modes) mainly probe the energy and damping of the interaction between the adsorbate and substrates. Parallel modes (T-modes) probe the curvature of the adsorbate-substrate interaction potential and the commensurability between adsorbate and substrate (Bruch and Hansen, 1997) and (Braun *et al*., 1998). From the information given by the phonon dispersion curves and the line width of the adsorbate vibration gleaned from HAS and related spectroscopes, it should be possible to predict and explain the friction for a given adsorbate -substrate system. For example, since the line width of the adsorbate vibrations is linearly proportional to the friction coefficient, a broader line width should imply a higher friction system. Also the existence of a Brillouin-Zone-centre gap for parallel or perpendicular phonon modes indicate commensurability between the adsorbate and substrate, (Bruch and Hansen 1997).The existence and size of the zone-centre gap may therefore predict the degree of lattice match-up

that causes friction. Although the comparative magnitude of friction between adsorbates and substrates may be predictable, it is still difficult to determine whether the origins of friction for a given system is /are phononic or electronic. Further, well planned and controlled experiments are necessary to differentiate between phononic and electronic processes (Dinelli *et al*., 2002;
Doremus, 2002).

2.6 FRICTION ANISOTROPY

There has been much work done on commensurate and incommensurate frictional systems and friction anisotropy. When two surfaces are commensurate, their lattices match in perfect registry. Theoretically, it has been shown that commensurate systems can have as much as 14 orders of magnitude higher friction than corresponding incommensurate systems. The lower friction levels for incommensurate systems are due to the random positions of atoms with respect to each other on the mismatched lattices. Interfacial forces tend to cancel in this case, resulting in very low friction (Hirano *et al*.,1991; Shinjo and Hirano,1993). There are several experiments that reveal the effect of incommensurability on friction, although none have reported the phenomenal change in friction that is theoretically possible. Most of these studies focused on the adhesion and friction between like-materials or materials with similar lattice spacing and go from commensurate to

incommensurate by rotating the lattices with respect to one another. For example, a surface force apparatus(SFA) was employed to study the adhesion of mica surface in distilled water and aqueous potassium chloride (KCl) (McGuiggan and Isrealachvili, 1990). The results related the adhesion of mica surfaces to the alignment of the mica surfaces with respect to one another. The adhesion peaked at $\theta = 0$, 60, 120 and 180 degrees ($\theta = 0$ corresponds to matching lattices), following the six-fold symmetry of the mica lattice. A related study of mica surfaces linked the friction of mica surfaces to their relative orientation, (Hirano *et al.,* 1991). Friction tester similar to a surface force apparatus (SFA) was used to rub two mica surfaces in both an argon-purged dry atmosphere with the surface temperature of the mica heated above 100° C to prevent water adsorption. These measurements were then compared to ambient condition measurements with the mica surface temperatures held at 20ºC. In the argon-purged atmosphere, the friction reached maximum levels when the surfaces were commensurate ($\theta = 0$, 60, 120 and 180 degrees, $\theta = 0$ corresponds to matching lattices) and minimum levels, dropping by a factor of 4 when the surfaces were incommensurate ($\theta = 30$, 90 etc). In ambient conditions, the original anisotropy disappeared, however owing to the adsorption of water and other contaminants onto the mica surfaces. The result lent support to the idea that frictional anisotropy is purely a surface effect

(Smith *et al*., 1996; Gyalog and Thomas, 1997).

Scanning tunneling microscope (STM) was employed in utra-high vacuum to study the sliding of a tungsten wire tip surface on a planar silicon surface. Much like an AFM, the tungsten tip was rastered across the silicon surface and a displacement sensor was used to measure the bending of the tungsten wire caused by the friction between the two surfaces. Employing Hooke's law to extract the frictional force from the displacement of the tungsten tip, it was found that the frictional force of the two surfaces in commensurate contact was 8×10^{-8}N. The friction vanished when the surfaces were in incommensurate contact, within their resolution. (The resolution of the instrument was 3×10^{-9}N). Not all friction anisotropy can be related to surface commensurability (Shinjo and Hirano, 1993). In some experiments, friction anisotropy disappears at low loads when the surfaces are in elastic contact and is only present at high loads when the surfaces are in plastic contact. A typical example is an experiment that studied the friction between nickel (100) surfaces in UHV with and without adsorbed surface coatings of sulphur and ethanol (Hirano *et al.*, 1991; Scharf *et al*., 1998). The adsorbed coatings modified the surface lattice of the bare nickel, the sulphur surface is well-ordered with lattice vectors rotated 45 degrees with respect to the bulk nickel, and the adsorbed ethanol is not ordered. The friction in this study was anisotropic and related to the bulk lattice structure of the nickel. The static friction coefficient was found to be minimized (lower by a factor of 3-4) at a bulk lattice mismatch of $\theta =$

45 degrees, regardless of the modifications to the surface by monolayer's of atomic sulphur and up to 4 monolayers of adsorbed ethanol. Their results suggest that in some systems in plastic contact that the frictional anisotropy is related to deformation of the bulk material.

2.7: Static Friction

One of the most common everyday experiences with friction at the microscopic scale is the occurrence of static friction. The force to initiate motion (which itself is quite variable, depending for example on how long the two surfaces have been in contact) is virtually always larger than that required to keep an object in motion (Eldrid *et al*., 2007). A closely associated phenomenon is that of stick – slip friction, whereby for certain sliding speeds, the velocity – weakening dependence of the transition from static to sliding friction leads to repetitive sticking and sliping at the interface, producing the all-too familiar screeching noises associated with brakes. Although static friction is ubiquitous, it is notoriously difficult to explain at the macroscopic and microscopic length scales (Sundip *et al.,* 2007; Suman *et al*., 2007).

Static friction and stick-slip motion are also familiar occurrences in nanotribology. Static friction has frequently been measured with surface force apparatus (SFA). Atomic scale stick-slip friction was first measured in the AFM by

(Mate *et al*., 1987). Using an AFM with a tungsten probe on a graphite surface, it was found that the frictional force of the probe on the graphite had a periodicity of 2.5 angstroms, the same periodicity as the graphite surface. Since 1987, atomic scale stick-slip friction has been observed on many different materials
(Germann *et al.*, 1993). Atomic scale stick-slip friction can be interpreted as the tip and sample remaining in the minimum potential energy position until a sufficiently strong shear stress is applied to force the tip to move (Carpick and Salmeron 1997). Interestingly, such stick-slip behaviour has always been observed to occur with the periodicity of the substrate lattice, even when the lattice points have multiple atoms. For example, it is not possible to differentiate between the molybdenum and the sulphur atoms in a MoS_2 surface. The stick – slip periodicity measured by the LFM is 3.16 angstroms, which corresponds to the distance between MoS_2 molecules in the lattice (Fujisawa *et al.*,1994; Terada *et al*., 2000).

Static friction has never been evident in QCM measurements, both solid-solid and liquid – solid interfaces being well described by the viscous friction law which is parameterized at low velocities by friction proportional to velocity, V. Where V is the velocity of the object through the liquid. Given the differences in the sliding speeds, and geometries between QCM, SFA and AFM, there was some debate about the underlying reason for the lack of static friction in the QCM. A recent experiment explored this question (Mate *et al*., 1987). This experiment

focused on the fact that while both QCM and SFA measurements of the shearing of the liquid films reveal friction, static friction is present only in the SFA geometry. Employing a "blow-off experiment", it was explored whether the open geometry or much greater shear rates of the QCM could account for the difference in the observed behaviours. Nitrogen was blown across a liquid film confined in a narrow channel. The laminar flow conditions generated a shear stress on the liquid film at shear rates comparable to those in the SFA. The results yielded viscous friction, so it was concluded that confined geometries and not the shear rates of the SFA and AFM resulted in static friction, while unconfined geometries like the QCM and the "blow-off" experiment are characterized by the viscous friction law.

The results are consistent with recent computer simulation experiments (Muser and Robbins, 2000). The effects that mobile atoms between two contacting crystalline surfaces have on friction were studied. As stated already, commensurate crystalline surfaces are expected to have high friction, and they exhibit static friction with or without contaminant atoms between the surfaces. Incommensurate crystalline surfaces, however, have very low friction. In the real world, however, almost all contacting surfaces are expected to be incommensurate, so the existence of static friction is difficult to explain. Simulations of modeled sub-monolayer and mobile contaminant films between two incommensurate surfaces were carried out.

It was observed that the mobile molecules found small gaps between the surfaces. Any sliding of the two surfaces will constrict or reduce the gaps in which the mobile molecules settle (Muser and Robbins, 2000). The molecules therefore resist sliding motion until the shear stress exceeds some threshold value and they are displaced, resulting in the presence of static friction.

2.8: TOMLINSON MODEL

In Tomlinson model, the motion of the tip is influenced by both the interaction with the atomic lattice of the surface and the elastic deformations of the cantilever. The shape of the tip-surface potential v(r) depends on several factors such as the chemical composition of the materials in contact and the atomic arrangement of the tip end (Gnecco *et al.*, 2010). First, we look at the analysis as a one dimensional case considering a sinusoidal profile with the periodicity of the atomic lattice a and a peak-to-peak amplitude E_0. If the cantilever moves with a constant velocity v along the x-direction, the total energy of the system is

$$E_{tot}(x,t) = -\frac{E_0}{2}\cos\frac{2\pi x}{a} + \frac{1}{2}K_{eff}(vt-x)^2 \qquad (2.3)$$

K_{eff} = elastic spring constant, E_0 = maximum potential energy of the system.

Fig. 2.4 shows the energy profile E_{tot} (x,t) at two different instants.

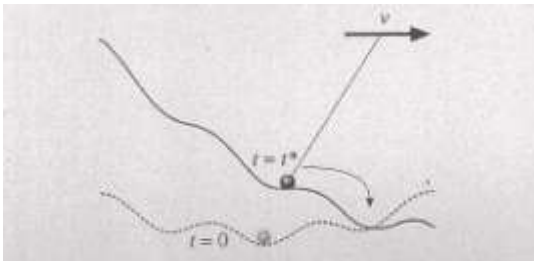

Fig. 2.4. Energy profile experienced by FFM tip, (black circle) at t = o (dotted line) and t = t (continuous line)* (Gnecco *et al.*, 2010).

When t = 0, the tip is localized in the absolute minimum of E_{tot}. This minimum increases with time due to the cantilever motion until the tip position becomes unstable when $t = t^*$ (Gnecco *et al.*, 2010). At a given time `t`, the position of the tip can be determined by equating to zero the first derivative of the expression E_{tot} (x,t) with respect to x to obtain

$$\frac{\partial E_{tot}}{\partial x} = \frac{\pi E_0}{a} \sin \frac{2\pi x}{a} - K_{eff}\,(vt-x) = 0 \qquad (2.4)$$

The critical position x^* corresponding to $t = t^*$ is determined by equating to zero the second derivative $\frac{\partial^2 E_{tot\,(x,t)}}{\partial x^2}$ to obtain

$$x^* = \frac{a}{2\pi} \arccos\left(-\frac{1}{y}\right) \qquad (2.5)$$

$$y = \frac{2\pi^2 Eo}{K_{eff}\, a^2} \qquad (2.6)$$

The coefficient y compares the strength of the interaction between tip and surface with the stiffness of the system. When t = t^*, the tip suddenly jumps into the next minimum of the potential profile. The lateral force F*

which induces the jump is given by (Gnecco *et al*, 2010)

$$F^* = \frac{K_{eff}}{2\pi} \; a\sqrt{y^2 - 1} \qquad (2.7)$$

Thus the stick-slip is observed only if y >1 i.e when the system is not too stiff or the tip-surface interaction is strong enough (Gnecco *et al.*, 2010).

Fig. 2.5 shows the lateral force F_L as a function of the cantilever position, x.

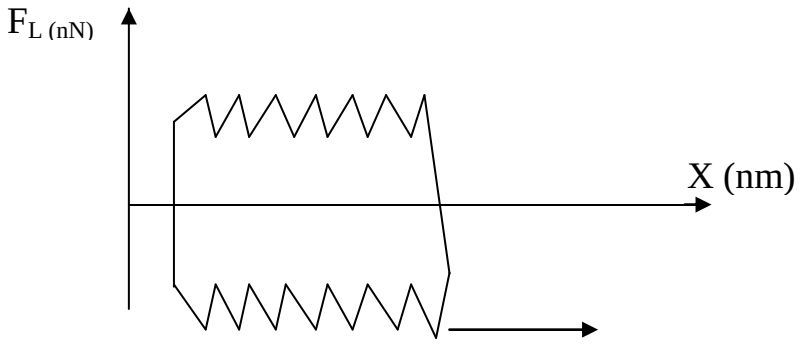

Fig. 2.5. Friction loop obtained by scanning back and forth in the one-dimensional Tomlinson models. The effective spring constant K_{eff} is the slope of the sticking part of the loop (if y>>1) (Gnecco *et al*., 2010).

When the cantilever is moved rightward, the lower part of the curve in Fig. 2.5 is obtained. If at a certain point, the cantilever's direction of motion is suddenly inverted, the force has the profile shown in the upper part of the curve. The area of

the friction loop obtained by scanning back and forth gives the total energy dissipated (Gnecco *et al.*, 2010).

Two-dimensional Tomlinson model:

In two dimensions, the energy of the system is given by

$$E_{tot}(r,t) = U(r) + \frac{K_{eff}}{2}(vt-r)^2 \qquad (2.8)$$

where r = (x,y) and v is arbitrarily oriented on the surface.

Figure 2.6 shows the regions for a potential of the form represented by equation (2.8).

The tip follows the cantilever adiabatically as long as it remains in the (++) – region. When the tip is dragged to the border of the region it suddenly jumps into the next (++) – region (Gnecco *et al.*, 2010).

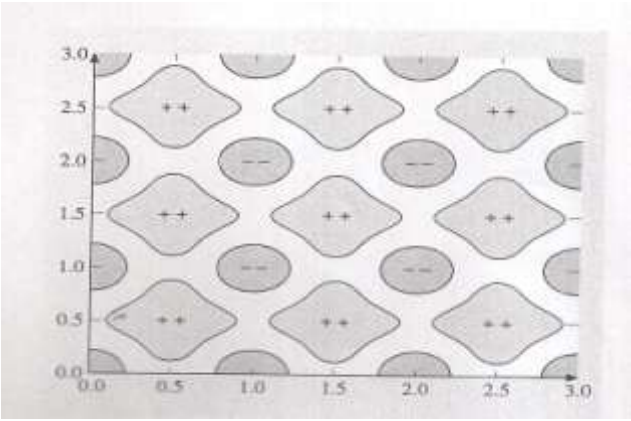

Fig 2.6: Regions of the tip plane labeled according to the signs of the eigenvalues (Gnecco *et al.*, 2010).

In the above discussions we assumed that the tip is terminated by only one atom. Let us consider the case of a periodic surface sliding on another periodic surface. The atoms of one surface are harmonically coupled with their nearest neighbours, (Gnecco *et al.*, 2010). We consider only the case of quadratic symmetries with lattice constants a_1 and a_2 for the upper and lower surfaces respectively. In such context, the role of commensurability is essential. Let the roots of the quadratic equation resulting from the quadratic symmetries be x_1 and x_2 , x_1 greater than x_2.

In one-dimension, It was predicted that friction should decrease with decreasing commensurability, the minimum of friction being reached when

$$\frac{a_1}{a_2} = x_1 \qquad (2.9)$$

and maximum friction is obtained when

$$\frac{a_1}{a_2} = x_2 \qquad (2.10)$$

In two - dimension, the case of $a_1 = a_2$, was studied with a misalignment between the two lattices given by an angle θ .When the sliding direction changes, friction also varies from ` minimum value corresponding to the sliding angle $\emptyset = \frac{\theta}{2}$ to a maximum value which is reached when $\emptyset = \frac{\theta}{2} + \frac{\pi}{4}$. The misfit angle θ is related with commensurability (Bhushan, 2010). Since the misfit angles giving rise to commensurable structure form a dense subset, the dependence of friction on

θ should be discontinuous. The numerical simulations performed by Gyalog are in agreement with the conclusion.

2.9: LINEAR COMBINATION OF ATOMIC ORBITALS.

Molecular orbitals were first introduced in 1927and 1928.

Linear combination of atomic orbitals (LCAO) was introduced in 1929 (Lernard-Jones, 1929). A ground-breaking paper presented by Lernard-Jones in 1929 showed how to derive the electronic structure of fluorine and oxygen molecules from quantum principles. This qualitative approach to molecular orbitals theory is part of the start of modern quantum science. A molecular orbital (MO) is a function describing the wave-like behaviour of an electron in a molecule. This function can be used to calculate chemical and physical properties such as the probability of finding an electron in any specific region. Molecular orbitals are usually constructed by combining atomic orbitals or hybrid orbitals from each atom of the molecule or other molecular orbitals from groups of atoms. Hence, molecular orbitals represent regions in a molecule where an electron is likely to be found. A molecular orbital can specify the electron configuration of a molecule, the spatial distribution and energy of one electron or a pair of electrons. A molecular orbital is represented as a linear combination of atomic orbitals

(the LCAO-MO method). They are invaluable in providing model of bonding in molecules, understood through molecular orbital theory. Most present-day computational methods begin by calculating the MOs of the system. A molecular orbital describes the behaviour of one electron in the electric field generated by the nuclei and some average distribution of the other electrons (Kutzelnigg, 1996).

Molecular orbitals arise from allowed interactions between atomic orbitals, which are allowed if the symmetries (determined from group theory) of the atomic orbitals are compatible with each other. Efficiency of atomic orbital interactions is determined from the overlap (a measure of how well two orbitals constructively interact with one another) between two atomic orbitals which is significant if the atomic orbitals are close in energy. Molecular orbitals can be obtained from the linear combination of atomic orbitals. The number of molecular orbitals that form must equal the number of atomic orbitals in the atoms being combined to form the molecule. Linear combinations of atomic orbitals can be used to estimate the molecular orbitals that are formed upon bonding between the molecules constituent atoms. Similar to an atomic orbital, a Schrodinger equation which describes the behaviour of an electron can be constructed for a molecular orbital as well. Linear combinations of atomic orbitals, or the sums and differences of the atomic wave-functions provide approximate solutions to the molecular Schrodinger equations.

For simple diatomic molecules the obtained wavefunctions are represented mathematically by the equation (Lernard-Jones, 1929)

$$\Psi = C_a\psi_a + C_b\psi_b \qquad (2.11)$$

$$\psi^* = C_a\psi_a - C_b\psi_b, \qquad (2.12)$$

where ψ and ψ^* are the molecular wave functions for the bonding and anti-bonding molecular orbitals, respectively, ψ_a and ψ_b are the atomic wavefunctions from the atoms a and b, respectively, and C_a and C_b are adjustable coefficients. These coefficients can be positive or negative depending on the energies and symmetries of the individual atomic orbitals. As the two atoms come closer together their atomic orbitals overlap to produce areas of high electron density, and as a consequence, molecular orbitals are formed between the two atoms. The atoms are held together by the electrostatic attraction between the positively charged nuclei and the negatively charged electrons occupying bonding molecular orbitals (Frexedas *et al*., 2002) .

2.10: BOND-ORBITAL MODEL

When atomic orbitals interact, the resulting molecular orbital can be of three types: bonding, anti-bonding and nonbonding. Bonding interactions between atomic orbitals are constructive (in-phase) interactions. Bonding molecular orbitals are lower in energy than the atomic orbitals that combine to

produce them. Anti-bonding interactions between atomic orbitals are destructive (out-of-phase) interactions. Anti-bonding molecular orbitals are higher in energy than the atomic orbitals that combine to produce them. Non-bonding molecular orbitals are the result of no interaction between atomic orbitals because of lack of compatible symmetries. Non-bonding molecular orbitals will have the same energy as the atomic orbitals of one of the atoms in the molecule

(Gary and Donald, 2004).

Later Harrison (Animalu, 1977) developed a new model of partial covalency in binary AB compounds starting from an atomic-like bond-orbital model rather than Philips band-like dielectric model. Harrison`s argument is that in the extreme ionic limit as one expects in large band gap instructors of the rock salt family like MgO having full inert gas configuration on the anion, a localized electron (bond) picture provide a more physical representation of the electronic states than the itinerant-electron (band) picture of the dielectric model. In the bond-orbital model, a hybrid orbital h^a is constructed from the atomic s and p orbitals centered on atom A and similar h^b is constructed from the atomic s and p orbitals centered

on atom B (Animalu, 1977).

$$h^a = \frac{1}{2}\ (s^a + \sqrt{3}\ p^a) \qquad (2.13)$$

$$h^b = \frac{1}{2}\ (s^b + \sqrt{3}\ p^b). \qquad (2.14)$$

In terms of these, the two parameters of the model are defined namely the covalency energy (V_2) and the polarity energy (V_3) related to the ionicity energy but not equivalent to it given by

$$2V_2 = - (<h^b|H|h^a> + < h^a|H|h^b>) \quad (2.15)$$

and

$$2V_3 = (< h^b|H|h^b> - < h^a|H|h^a>), \quad (2.16)$$

where H is the one-electron Hamiltonian of the AB system. To relate V_2 and V_3 to the gap between bonding (valence) and anti-bonding (conduction) bands, we define the molecular orbitals

$$\psi_A = \sqrt{½} (h^a - ih^b), \quad (2.17)$$

$$\psi_B = \sqrt{½} (ih^a + h^b) \quad (2.18)$$

which are normalized and have an overlap with real and imaginary parts.

$$<\psi_A|\psi_B> = \frac{1}{2} i (<h^a|h^a> - <h^b|h^b>) + \frac{1}{2} (<h^a|h^b> + <h^b|h^a>) \quad (2.19)$$

If $<h^a|h^a> = <h^b|h^b>$, the imaginary (polar) term drops and we have

$$<\psi_A|\psi_B> = \frac{1}{2} (<h^a|h^b> + <h^b|h^a>) \quad (2.20)$$

But if $<h^a|h^a> \neq <h^b|h^b>$ then the overlap wave function contains both the polar and covalent components.

Then the energy gap

$$E_g = (V_2^2 + V_3^2)^{½} \quad (2.21)$$

is given by

$$\langle \psi_A|H|\psi_B\rangle = \frac{1}{2}(\langle h^a|H|h^b\rangle + \langle h^b|H|h^a\rangle)$$

$$+\frac{1}{2}\, i(\langle h^a|H|h^a\rangle - \langle h^b|H|h^b\rangle) = -(V_2 + i\, V_3) \qquad (2.22)$$

In terms of these parameters, the fractional covalency (α_c) and polarity (α_p) are

$$\alpha_c = \frac{V_2}{(V_2^2 + V_3^2)^{1/2}} \qquad (2.23)$$

$$\alpha_p = \frac{V_3}{(V_2^2 + V_3^2)^{1/2}} \qquad (2.24)$$

and obey the relation

$$\alpha_c^2 + \alpha_p^2 = 1 \qquad (2.25)$$

The ionicity f_i of the dielectric model is related to α_p by (Ammalu,1977)

$$f_i = 1 - (1 - \alpha_p^2)^{3/2} \qquad (2.26)$$

Two models – the valence bond model and the molecular orbital model (Kutzelnigg, 1996) were developed almost simultaneously. Linus Pauling became the champion of the valence bond model. This model is essentially a quantum mechanical version of the electron-dot model. It attempts to describe what orbitals are used by each atom when electrons are shared. For example when the simple molecule of hydrogen (H_2) is formed from hydrogen atom, the valence bond model says that an s-orbital of one atom overlaps with an s-orbital of the other to form a bond. The molecular orbital model takes a different approach. It utilizes all of the orbitals on all of the atoms to generate a set of molecular orbitals.

2.11: TEMPERATURE DEPENDENCE OF NANOTRIBOLOGY.

From Tomlinson model, at a given time $t < t^*$, the tip jump is prevented by the energy barrier $\Delta E = E(X_{max}, t) - E(X_{min}, t)$, where X_{max}. corresponds to the first maximum observed in the energy profile and X_{min} is the actual position of the tip. The quantity ΔE decreases with time or equivalently with the frictional force F_L until it vanishes when $F_L = F^*$. Close to the critical point, the energy barrier can be written approximately as (Gnecco et al, 2010)

$$\Delta E = \mu(\bar{F} - F_L) \qquad (2.27)$$

where $\bar{F}$ is close to the critical value F^* .

At finite temperature, the lateral force required to induce a jump is lower than F^*. To estimate the most probable value of F_L at this point, we consider the probability `P` that the tip does not jump. This probability changes with time `t` according to the master equation (Gnecco et al, 2010)

$$\frac{dp(t)}{dt} = -f_o \exp\left(\frac{-\Delta E(t)}{K_B T}\right) P(t) \qquad (2.28)$$

where f_o is the characteristic frequency of the system.

If time is replaced by the corresponding lateral force, the master equation becomes (Gnecco *et al.*, 2010).

$$\frac{dp(F_L)}{dF_L} = -f_o \exp\left(\frac{-\Delta E(F_L)}{K_B T}\right) (P(F_L) \qquad (2.29)$$

The above equation shows that the probability of a tip jump is reduced at low temperatures T until it vanishes when T = 0. This predicts that friction should change with temperature. Using FFM, the effects of temperature on the nanotribology of n-hexadecane and octamethyllyclo-tetrasiloxane were studied. The results in both cases show that nanotribology decreases with increase in temperature (Bhushan, 2010).

The effect of temperature on friction and adhesion was studied using a thermal stage attached to the AFM. The friction force was measured at increasing temperature from 22 - 125°C. The results show that the increasing temperature causes a decrease of friction force adhesive force and coefficient of friction of Si(100), Z-15 (lubricant) and Z-DOL (BW) (lubricant) (Bhushan, 2010). This can be explained from the fact that at high temperature, desorption of water leads to the decrease of friction force, adhesive force and coefficient of friction of all the samples. Besides that, the reduction of surface tension of water also contributes to the decrease of friction and adhesion. For Z-15 film, the reduction of viscosity at high temperature has an additional contribution to the decrease of friction. In the case of Z-DOL (BW) film, molecules are more easily oriented at high temperature which may also be responsible for the low friction. Using a surface force apparatus, it has been shown that a change in temperature induces phase

transformation (from crystalline, solid-like to amorphous, liquid like) in surfactant monolayers, which are responsible for the observed changes in friction force.

Tomlinson`s model was used to study the temperature dependence of nanotribology on n-hexadecane and octamethycyclotetrasiloxane and in each case, the results show that friction force decreases as temperature increases,

(Gnecco *et al*, 2010). The effects of temperature on viscosity of silica was studied. The experimental results show that viscosity decreases as temperature increases.

The effects of temperature on nanotribology of sodium chloride, NaCl (001) was studied using FFM with silicon tip. The measurement was carried out under ultrahigh vacuum and low temperature regime. The results indicate that nanotribology decreases with increase in temperature (Krylov and Frenken, 2014). Hence at low velocity regime, temperature acts as a lubricant. Thermally activated stick-slip results in a strong decrease of nanotribology with increase in temperature. A significant decrease of nano-friction with increase in temperature was observed in a series of AFM measurements on graphite in ultrahigh vacuum (UHV) conditions and in a wide temperature range (140-750k) (Gnecco and Meyer, 2015). In another series of UHV experiments, the temperature dependence of nanotribology was measured from cryogenic conditions to a few hundred Kelvin for silicon, silicon carbide (SiC), ionic crystals and graphite. The results indicate

that nanotribology decreases with increase in temperature (Gnecco and Meyer, 2015).

2.12: VELOCITY DEPENDENCE OF NANOTRIBOLOGY

Velocity dependence of nanotribology was studied using FFM. It was observed that friction between silicon tips and diamond, graphite or amorphous carbon is constant with scan velocities of few μm/s. In experiments on lipid films on mica, a range of velocities from 0.01 to 50μm/s was explored and a critical velocity V_c = 3.5 μm/s was found which discriminates between an increasing friction and a constant friction (Liu and Bhushan, 2004).

In investigating the velocity effect on nanotribology, the friction force versus normal load relationships of Si (100), Z-15 and Z-DOL (BW) at different velocities were measured (Bhushan, 2010; Sundararajan and Bhushan, 2000). The results indicate that for silicon wafer, the friction force decreases logarithmically with increasing velocity. For Z-15, the friction force decreases with increasing velocity up to 10μm/s after which it remains almost constant. The velocity has a much smaller effect on the friction force of Z-DOL (BW). It reduced slightly only at very high velocities. The results also indicate that the adhesive force of Si (100) is increased when the velocity is higher than10μm/s. The adhesive force of Z-15 is reduced dramatically when the velocity increased up to 20μm/s, after which it is reduced slightly. The adhesive force of Z-DOL (BW) also decreased at high

velocity. In the testing range of velocity, only the coefficient of friction of Si (100) decreases with velocity, but the coefficient of friction of Z-15 and Z-DOL (BW) almost remain constant. This implies that the friction mechanism of Z-15 and Z-DOL (BW) do not change with variations in velocity. The mechanisms of the effect of velocity on the adhesions and friction are explained based on the tribochemical reactions. For Si (100), tribochemical reaction plays a major role. Although at high velocity, the meniscus is broken and does not have enough time to rebuild, the contact stresses and high velocity lead to tribochemical reactions of Si (100), water and $Si_3 N_4$ tip, which have native oxide (SiO_2) layers with wafer molecule (Gnecco *et al.*, 2010). The following reactions occur.

$$SiO_2 + 2H_2O \longrightarrow Si(OH)_4 \qquad (2.30)$$

$$S i_3 N_4 + 16H_2O \longrightarrow Si_3(OH)_4 + 4(NH_4O_3H_3) \qquad (2.31)$$

The $Si(OH)_4$ is removed and continuously replenished during sliding. The $Si(OH)_4$ layer between the tip and Si (100) surface is known to be of low shear strength and causes a decrease in friction force and coefficient of friction in the lateral direction. The chemical bonds of SiOH between the tip and Si (100) surface induce large adhesive force in the normal direction. For Z-15 film, at high velocity, the meniscus formed by condensed water and Z-15 films molecules is broken and does not have enough time to rebuild. Therefore the adhesive force and consequently, the friction force is reduced. For Z-DOL (BW) film, the surface can absorb few

water molecules in ambient condition and at high velocity. These molecules are displaced which is responsible for a slight decrease in friction force and adhesive force. Even at high velocity range, the friction mechanisms for Z-15 and Z-DOL (BW) films still are shearing of the viscous liquid and molecular orientation, respectively. Thus the coefficients of friction of Z-15 and Z-DOL (BW) do not change with velocity. It was suggested that in the case of samples with mobile films, such as condensed water and Z-15 films, alignment of liquid molecules (shear thinning) is responsible for the drop in friction force with an increase in scanning velocity. This could be another reason for the decrease in friction force with velocity for Si(100) and Z-15 film in the study (Bhushan and Liu, 2004).

Experiments have demonstrated that capillary condensation can lead to a logarithmic decrease of nano-friction with increasing velocity (Krylov and Frenken, 2014). This has been interpreted as the consequence of the thermally activated nucleation of water bridges between tip and sample asperities, in a dynamics that somewhat resembles the velocity weakening observed in macroscale contacts. Measurements of nanotribology of surfaces modified so that they can form hydrogen-bonding networks also show a reduction of nano-friction with increasing sliding velocity which has been explained analogously, in terms of the formation and rupture of these bonding networks (Krylov and Frenken, 2014).

The variation of nano-friction as a function of sliding velocity was studied using AFM with silicon tip on NaCl (100). Under a humid environment, nanotribology decreases with increase in velocity (Gnecco and Meyer, 2015). This can be attributed to the formation of water menisci by thermally activated capillary condensation. This decrease of nano-friction with velocity increase can also be associated with chemical modifications. This happens in systems forming cross-links structure that can be broken by the applied load, such as surfaces terminated by -OH,-COOH and -NH_2 groups. At slow velocities, there is more time to form bonds between tip and surface, which results in larger nano-friction (Gnecco and Meyer, 2015). If the scan velocity increases, thermally activated processes are less important, and beyond a critical value, the nano-friction becomes independent of the velocity as seen in a series of measurements between silicon tips and diamond, graphite and amorphous carbon surfaces with scan velocities above 1μm/s (Gnecco and Meyer, 2015). The dependence of nanotribology on the sliding velocity was studied using AFM tip sliding on graphene membrane. The results show that nanotribology increases with decrease in velocity (Sandoz-Rosado, 2013).

2.13: LOAD DEPENDENCE OF NANOTRIBOLOGY

When there is no adhesive force between two surfaces, the only attractive force that needs to be overcome for sliding to occur is the externally applied load or pressure. It is instructive to compare the magnitudes of the externally applied pressure to the internal Van der Waals pressure between two smooth surfaces. The internal Van der waals pressure between two flat surfaces is given by

$$P = \frac{A_H}{6\pi D_0^3} \qquad (2.32)$$

Using a typical Hamaker constant of $A_H = 10^{-19}$ J and assuming D_o = 2nm for the equilibrium interatomic spacing we have P = 1 GPa (10^4 atm.) (Isrealachvili and Ruths, 2010).

This implies that we should not expect the externally applied load to affect the interfacial friction force until the externally applied load begins to exceed

$\approx$ 100MPa (10^3 atm). This is in agreement with experimental data where the effect of load became dominant at pressures in excess of 10^3atm. This actually implies that the effect of normal load on nano-friction becomes dominant at high values of load (Isealachvili and Ruths, 2010). Nanotribological properties of Si (100), Z-15 and Z-DOL (BW) films on silicon (100) was investigated. The friction force versus normal load curves were measured by making friction force measurements at increasing normal loads (Liu and Bhushan, 2004). The results obtained for silicon (100), Z-15 and Z-DOL (BW) films on Si (100) are shown in Fig. 2.7.

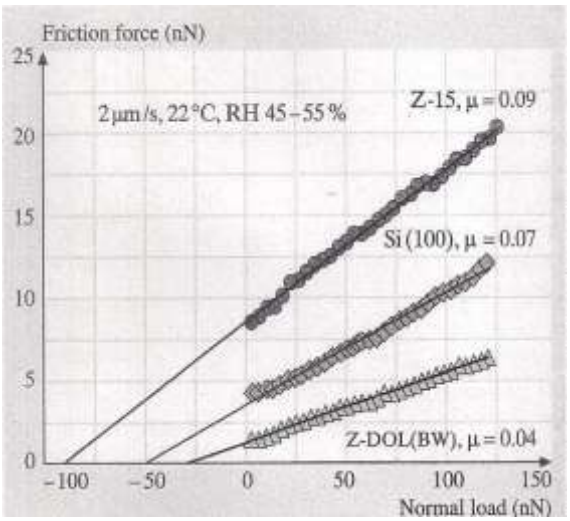

Fig 2.7: Friction force versus normal load curves for Si (100), 2.8nm – thick, Z-15 film and 2.3nm-thick Z-DOL (BW) film at 2μm/s and in ambient air sliding against a Si_3N_4 tip (Liu and Bhushan, 2004).

An approximately liner response of all three samples is observed in the load range of 5-130nN. The friction force of solid-like Z-DOL (BW) is consistently smaller than that for Si (100), but the friction force of liquid – like Z-15 lubricant is higher than that of Si (100). In the above figure the nonzero value of friction force at zero external load is due to the adhesive forces (Liu and Bhushan, 2004). The static friction force of silicon micromotors lubricated with Z-DOL was studied using AFM. It was found that liquid-like lubricants of Z-DOL significantly increases the static friction force whereas solid-like Z-DOL (BW) coating can dramatically reduce the static friction force. In both cases, the results show that friction increases with increase in normal load (Sundararajan and Bhushan, 2001).

Friction versus load in ambient air (RH-55%) was measured with a silicon tip on C_{6o} islands grown on a germanium sulphide (GeS) substrate. Since the C_{6o} coverage was incomplete, the experiment on friction measurements was performed with the same tip on both the GeS and the C_{6o} surfaces together (Carpick and Salmeron, 1997). In both cases, the results show that friction increases with increase in normal load. The load dependence on nanotribology of C_{6o} was studied using atomic force microscope at different temperatures. The results show that nanotribology increases with increase in normal load (Liang *et al*., 2003). The effects of normal load on nanotribology of sodium chloride NaCl(001) was studied using FFM with silicon tip. The results show that nanotribology increases with increase in normal load (Krylov and Frenken, 2014). Their results also show that nano- friction nearly disappears at low loads.

The general trend observed in AFM experiments is that nanotribology increases with increase in normal load (Gnecco and Meyer, 2015). A linear load dependence of nanotribology was reported on various substrates including gold and alkylthiol molecules (Gnecco and Meyer, 2015). The variation of friction with normal load for aluminum-aluminum pair, aluminum-copper pair and aluminum-brass pair were studied. The results show that friction coefficient increases with increase in normal load. This may be due to increase in the adhesion strength, (Nuruzzaman and Chowdhury, 2012). At low loads, the oxide film effectively

separates two metal surfaces and there is little or no true metallic contact, hence, the friction coefficient is low. At higher load conditions, the film breaks down resulting in intimate metallic contact which is responsible for higher friction, (Nuruzzamn and Chowdhury, 2012). Effects of normal load on nanotribology of various forms of human hair were studied using AFM. The results indicate that nanotribology increases with increase in normal load (Bhushan and La Torre, 2010). Normal load dependence of nanotribology was studied for silicon dioxide (SiO_2) and graphene using AFM. The results show that nanotribology increases with increase in normal load with graphene having low friction when compared to silicon dioxide substrate (Sandoz-Roszdo, 2013).

2.14 APPLICATIONS

Nanotribological properties of materials can be applied in the following areas:

- Information storage systems in computers.
- Information storage systems in mobile phones.
- Mobile phone ear-piece and mouth-piece
- Radar control systems.
- Autotronic components e.g. monitors, sensors etc.
- Mechatronic components in industrial robotic machines.
- Designing of automobile break systems and preparation of lubricants

CHAPTER THREE

MATERIALS AND METHODS

3.1 MODELS

The models developed and used for this work are of six different types. Jump energy quantum models for high and low ionic energy gaps were developed through a combination of bond – orbital model and Tomlinson's model. Temperature model was developed through derivation of an equation for lateral force (friction force) F_L using Tomlinson's model and Sang's` equation. This derived equation was carefully modified so that it can be applied over a wide range of semiconductors including binary compounds. Low and high velocity models were developed through a transformation and modification of temperature model. Normal load model was developed through a transformation and modification of temperature model. It should be noted that bond-orbital model is an instrument for structural analysis and nanotribology is a structural problem, hence, the choice of bond-orbital model in this work.

3.2 DEVELOPMENT OF JUMP ENERGY QUANTUM MODELS FOR HIGH AND LOW IONIC ENERGY GAPS

From Tomlinson's model, (Gnecco et al, 2010) the equation describing the thermal effects on atomic friction is given by

$$\frac{dp(t)}{dt} = - f_o \exp\left(-\frac{\Delta E(t)}{K_\beta T}\right) P(t) \quad (3.1)$$

where f_o is the characteristic frequency of the system. If we replace time with the lateral force F_L we have

$$\frac{dp(F_L)}{dF_L} = - f_o \exp\left(-\frac{\Delta E(F_L)}{K_\beta T}\right) P(F_L) . \quad (3.2)$$

From this model, the force preventing the tips jump is ΔE which is the energy barrier. This is given by

$$\Delta E = E(X_{max}, t) - E(X_{min}, t), \quad (3.3)$$

where X_{max} corresponds to the first maximum observed in the energy profile and X_{min} is the actual position of the tip. Close to the critical point, the energy barrier can be written approximately as

$$\Delta E = \mu (\overline{F} - F_L) \quad (3.4)$$

where $\overline{F}$ is close to the critical value F^*

In terms of the lattice parameter a, the energy barrier ΔE (Gnecco *et al*., 2010) is given by

$$\Delta \boldsymbol{E} = \frac{\hbar^2}{2m} \left(\frac{2\pi}{a}\right)^2 . \quad (3.5)$$

Simplifying equation (3.5) we have

$$\Delta \boldsymbol{E} = \frac{h^2}{2m} \frac{1}{a^2} \quad (3.6)$$

In bond –orbital model in binary compounds, if the imaginary (polar) components and real (covalent) components are present, then the bond energy gap is

$$E_g = -(V_2 + iV_3) \quad (3.7)$$

but if the imaginary (polar) part vanishes, then the overlap wave function contains only the covalent (real) part (Animalu, 1997) so that the magnitude of E_g is

$$E_g = (V_2^2 + V_3^2)^{½} \quad (3.8)$$

Using equation (3.7), $\Delta \boldsymbol{E} = E_T$ was calculated for Si, Ge, Sn, ZnS, CdS, ZnSe and CdSe. Comparing the results obtained, we found that the calculated values of $\Delta \boldsymbol{E} = E_T$ using Tomlinson's model is related to E_g (from bond-orbital model) by the equation

$$E_{TS} = \beta\left[E_g - \left(\propto_c^{½} + f_i^2\right)\right], \quad (3.9)$$

for $\alpha_c \geq 3.85$ eV.

α_c is the ionic energy gap, f_i is the ionicity of the material' and β is an empirical constant with the value

$\beta = 1.073$

If $\alpha_c < 3.85$eV, then another equation holds for E_{TS} and is given by

$$E_{TS} = \beta\,(E_g - f_i^{½}) \quad (3.10)$$

Equations (3.9) and (3.10) are jump energy quantum models for high and low ionic energy gaps respectively which we developed. Jump energy quantum model for low ionic energy gap was used to generate results for silicon (Si), germanium (Ge) and Tin (Sn), while jump energy quantum model for high ionic energy gap was

used to generate results for zinc sulphide (ZnS), cadmium sulphide (CdS), zinc selenide (ZnSe) and cadmium selenide (CdSe).

3.3 DEVELOPMENT OF TEMPERATURE MODEL

In pure practical works in nanotribology research, the major equipment which makes this work possible is Atomic Force Microscope (AFM) and Friction Force Microscope (FFM). In each case, the major thing that generates readings is the movement of the tip on a given sample (material). From Tomlinson's model, the motion of the tip is influenced by

(1) The interaction with the atomic lattice of the surface.

(2) The elastic deformation of the cantilever.

If the cantilever moves with a constant velocity (v) in x-direction the total energy of the system is

$$E_{tot}(x, t) = -\frac{E_0}{2}\cos\frac{2\pi X}{a} + \tfrac{1}{2}K_{eff}(vt-x)^2 \qquad (3.11)$$

At any time't', the position of the tip can be determined by equating to zero the first derivative of the expression E_{tot} (x, t) with respect to x to obtain

$$\frac{dE_{tot}}{dx} = \frac{\pi E_0}{a}\sin\frac{2\pi x}{a} - K_{eff}(vt-x) = 0 \qquad (3.12)$$

The critical position x^* corresponding to $t = t^*$ is determined by equating to zero the second derivative of E_{tot} (x, t) which gives

$$x^* = \frac{a}{2\pi} \arccos\left(-\frac{1}{y}\right) \quad (3.13)$$

$$y = \frac{2\pi^2 E_O}{K_{eff}\, a^2} \quad (3.14)$$

When $t = t^*$, the tip suddenly jumps into the next minimum of the potential profile. The lateral force F^* which induces the jump is given by (Gnecco *et al.*, 2010)

$$F^* = K_{eff} \frac{a}{2\pi} \sqrt{y^2 - 1} \quad (3.15)$$

Therefore, the stick-slip is observed only when $y > 1$ i.e only when the system is not too stiff.

In two dimensions, the energy of the system is

$$E_{tot}(r, t) = U(r) + \frac{K_{eff}}{2} (Vt - r)^2 \quad (3.16)$$

Using the assumption that $y >> 1$ at a given time $t = t^*$, the tip jump is prevented by the energy barrier $\Delta \boldsymbol{E}$. $\Delta \boldsymbol{E}$ decreases with increasing frictional force F_L until it vanishes when $F_L = F^*$.

It was observed that the energy barrier ΔE close to the critical point is better approximated by the relation (Gnecco *et al.*, 2010)

$$\Delta \boldsymbol{E} = \mu (F^* - F_L)^{3/2} \quad . \quad (3.17)$$

This equation is Sang's equation

Where $\mu = 0.01$ (Gnecco *et al.*, 2010) .

Tomlinson gave the logarithmic dependence of his model as

$$\mu \frac{(F^* - F_L)^{3/2}}{k_B T} = \text{In} \frac{V_c}{V} - \text{In} \sqrt{1 - \frac{F^*}{F_L}} \quad (3.18)$$

Where v_c is a critical velocity and v is any velocity of tip (Gnecco *et al.*, 2010)

If $v << v_c$ then the second logarithm in equation (3.18) can be neglected to obtain

$$F_L = F^* - \left(\frac{k_B T}{\mu}\right)^{2/3} \left(\text{In} \frac{V_c}{V}\right)^{2/3}. \quad (3.19)$$

If we take value of v such that $\frac{V_c}{V} = e$, the velocity effect on F_L is kept constant and equation (3.19) becomes

$$F_L = F^* - \left(\frac{k_B T}{\mu}\right)^{2/3}. \quad (3.20)$$

Rearranging equation (3.17) we have

$$F_L = F^* - \left(\frac{\Delta E}{\mu}\right)^{2/3}. \quad (3.21)$$

Adding (3.20) and (3.21) we obtain

$$F_L = F^* - \tfrac{1}{2} \left[\left(\frac{\Delta E}{\mu}\right)^{2/3} + \left(\frac{k_B T}{\mu}\right)^{2/3}\right]. \quad (3.22)$$

After series of work with equation (3.22), we carefully modified it based on the fact that temperature effect on nanotribology requires a more sensitive equation which will predict experimental results more accurately. In modifying the above equation, we note that multipliers and origin shifters help to enhance the sensitivity of models. These multipliers and origin shifters are called normalization constants and their exact values were determined through a process of fitting. These modifications led to the equation

$$F_L = F^* - \frac{P^2T^2}{2}\left[\left(\frac{\Delta E}{\mu}\right)^{2/3} + \frac{1}{\mu}\left(\frac{k_B T^2}{\mu}\right)^{2/3}\right]. \quad (3.23)$$

Where P which is an empirical constant is given by

P = (R+X).

R = 1.38×10^{-3} and X = $(n_i - 1) \times 10^{-3}$

n_i takes values from 1-4.

k_B = Boltzmann's constant

T = Temperature

μ= Empirical constant

F* = Force that induces tips jump

Equation (3.23) is the temperature model which we developed.

When the normalization constants were inserted and the model tested, its ability to reproduce experimental results shows the correctness of the constants.

This equation was used to study the effect of temperature on nanotribology of Si, Ge, Sn, ZnS, CdS, ZnSe and CdSe and results generated.

F^* for each semiconductor was calculated using equation (3.15), noting that

K_{eff} = 1.0.

After series of work with y, we adopted y = 100 to satisfy the condition that y>1.

3.4 DEVELOPMENT OF LOW AND HIGH VELOCITY MODELS

In developing these models, the parameter of interest is velocity. To do this, we go back to temperature model which is

$F_L = F^* - \frac{P^2T^2}{2}\left[\left(\frac{\Delta E}{\mu}\right)^{2/3} + \frac{1}{\mu}\left(\frac{k_B T^2}{\mu}\right)^{2/3}\right]$.

Since this model contains $\Delta \boldsymbol{E}$ which has a very essential property of crystals i.e lattice spacing, the velocity models can be obtained by modification of the above equation.

Dropping $\frac{P^2T^2}{2}$ in the above model we have

$$F_L = F^* - \left[\left(\frac{\Delta E}{\mu}\right)^{2/3} + \frac{1}{\mu}\left(\frac{k_B T^2}{\mu}\right)^{2/3}\right] \quad (3.24)$$

Substituting v for T in equation (3.24) and introducing the necessary constants, we have

$$F_L = \alpha_v F^* - \left[\left(\frac{\Delta E}{\mu}\right)^{2/3} + \left(\frac{k_B V^2}{\mu^3}\right)^{2/3} \frac{1}{K}\right]. \quad (3.25)$$

Where α_v and K are constants given by

$\alpha_v = 1.043$ and

$K = 1.0 \times 10^{-10}$

Equation (3.26) holds for

$v \leq 2.0\mu m/s$.

If $v > 2.0\mu m/s$ then another equation holds and is obtained by introducing another

constant C to obtain

$$F_L = \alpha_v F^* - [\,[(\tfrac{\Delta E}{\mu})^{2/3} + (\tfrac{k_B V^3}{\mu^3})^{2/3}\tfrac{1}{K}] + C\,] \qquad (3.26)$$

Where C is another constant given by C = 2.22×10^{-9}N

Hence equations (3.25) and (3.26) are low and high velocity models respectively which we developed.

These models were used to study the effects of velocity on the nanotribology of the seven semiconductors under study – Si, Ge, Sn, ZnS, CdS, ZnSe and CdSe.

Results were generated and presented in the graphs.

3.5 DEVELOPMENT OF NORMAL LOAD MODEL

In developing this model, the parameter of interest is Normal Load. To develop a model for studying the effect of normal load on nanotribology of semiconductor surfaces we go back to equation (3.24) which is the temperature model.

$$F_L = F^* - \tfrac{P^2T^2}{2}\,[\,(\tfrac{\Delta E}{\mu})^{2/3} + \tfrac{1}{\mu}(\tfrac{k_B T^2}{\mu})^{2/3}]$$

Removing $\frac{P^2T^2}{2}$ and substituting L for T^2 in above model, we obtain

$$F_L = F^* - [(\tfrac{\Delta E}{\mu})^{2/3} + \tfrac{1}{\mu}(\tfrac{k_B L}{\mu})^{2/3}] \qquad (3.27)$$

Modifying further and introducing the necessary constants, we have

$$F_L = \tfrac{F^*}{2} + [(\tfrac{\Delta E}{\mu})^{2/3} + (\tfrac{k_B L}{\mu^3})^{2/3}\tfrac{1}{M}] + N \qquad (3.28)$$

where M and N are constants.

$M = 1.0 \times 10^{-7}$

$N = (n_i - 1) \times 10^{-9}$ N

and $n_i = 1, 2, 3\ldots\ldots$

Hence equation (3.28) is normal load model which was developed. This model was used to study the effects of normal load (L) on the nanotribology of the seven semiconductors under study and results were generated and presented in graphs.

HAPTER FOUR

RESULTS AND DISCUSSIONS

4.1 RESULTS OBTAINED WITH JUMP ENERGY QUANTUM MODELS FOR HIGH AND LOW IONIC ENERGY GAPS

Jump energy quantum models for high and low ionic energy gaps were used to generate results for the seven semiconductors under study. The results obtained are presented in Table 1.

Table 1: Results obtained using jump energy quantum models for high and low ionic energy gaps.

Material	Lattice Spacing a (A^o)	Average bond energy gap E_g(eV)	Calculated values of $\Delta E = E_T$ using Tomlinson model (eV)	Calculated values of $\Delta E = E_{Ts}$ using jump energy quantum models (eV)
Si	5.42	4.77	5.12	5.12
Ge	5.62	4.31	4.76	4.62
Sn	6.46	3.06	3.60	3.28
ZnS	5.41	7.85	5.14	5.33
CdS	5.83	7.11	4.43	4.52
ZnSe	5.67	7.05	4.68	4.60
CdSe	6.05	6.58	4.12	4.02

The results above show that the values obtained using equations (3.9) and (3.10) compare favourably with that abstained using Tomlinson model. Hence with equations (3.9) and (3.10), bond energy gap of every material which is obtained from bond – orbital model can be used to calculate ΔE for the material which is the energy that prevents the tip jump. The above results show that zinc sulphide has the highest value of ΔE among the semiconductors under study followed by Si, Ge, ZnSe, CdS, CdSe and Sn.

Since ΔE decreases with increasing frictional force, it follows that zinc sulphide exhibits better tribological properties at nano-level than other materials under study followed by Si and others. It should be noted that bond-orbital model is an instrument for structural analysis and nanotribology is a structural problem. Hence $\Delta E = E_{TS}$ for each material from the above table was used in temperature model.

4.2 RESULTS OBTAINED FOR THE SEMICONDUCTORS UNDER STUDY USING TEMPERATURE MODEL.

This model was used to study the effects of temperature on nanotribology of the seven semiconductors under study. The results obtained for silicon together with experimental results found in literature (Gnecco *et al*., 2010) are presented in Figure. 4.1.

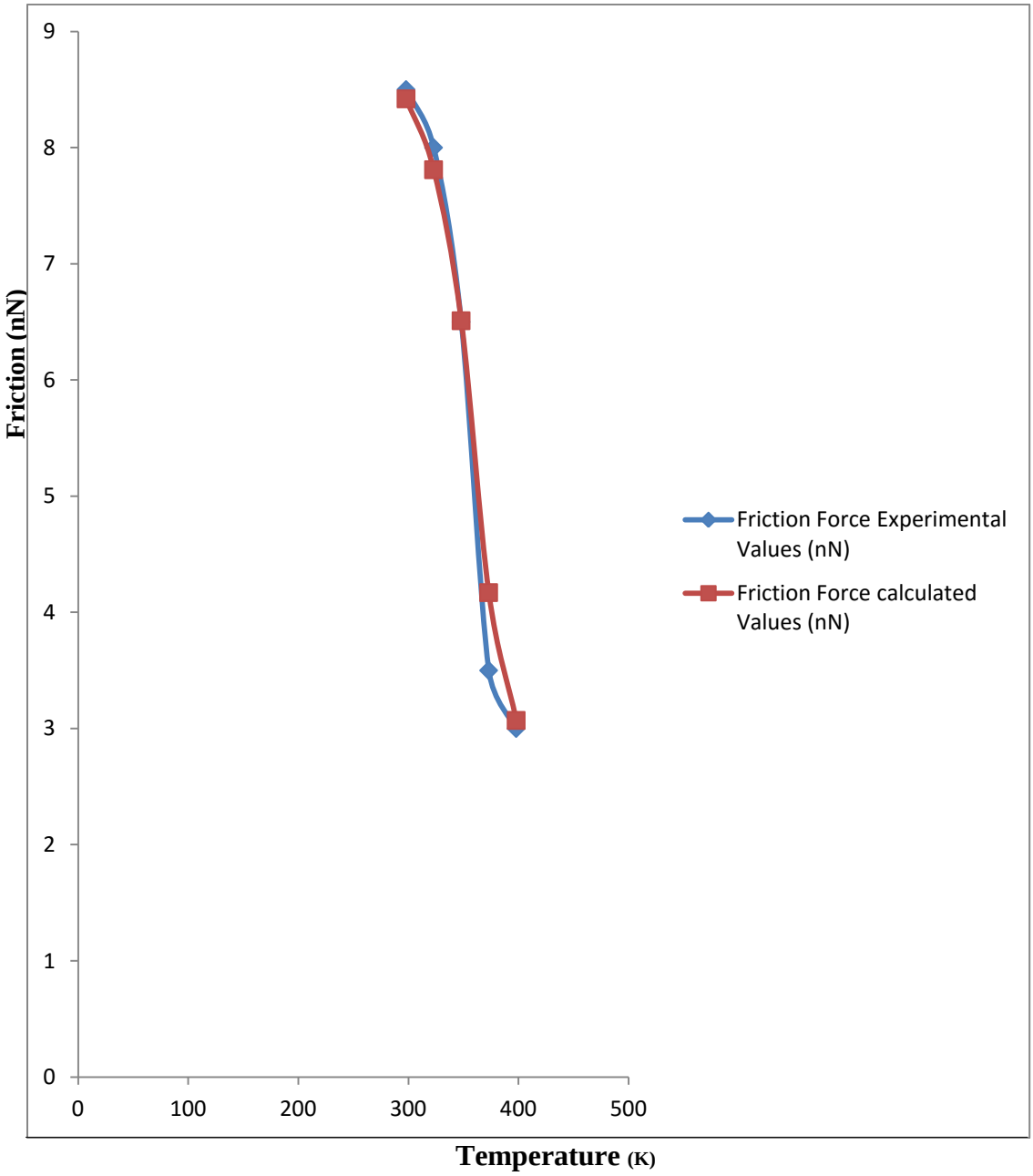

Fig. 4.1: Theoritical effects of temperature on nanotribology of Si compared with experimental results of Si

The above graphs show that the results obtained using the temperature model are in good agreement with experimental results of Si. The higher deviation observed in the two results at 373K could be attributed to the fact that in the graph of the experimental results , the point plotted for friction at 373K is the only point that falls well off the line of best fit. This is observed in the graph of the results as found in literature. Hence, this model can properly predict experimental results. The model was also used for other six semiconductors under study – Ge, Sn, Zns, Cds, ZnSe and Cdse and the results obtained are presented according to the groupings Ge and Sn, ZnS and CdS, ZnSe and CdSe in Figures 4.2, 4.3, and 4.4 respectively. The above grouping is based on the fact that Ge and Si are intrinsic semiconductors, both ZnS and CdS contain sulphur while the third group contain selenium as a common element.

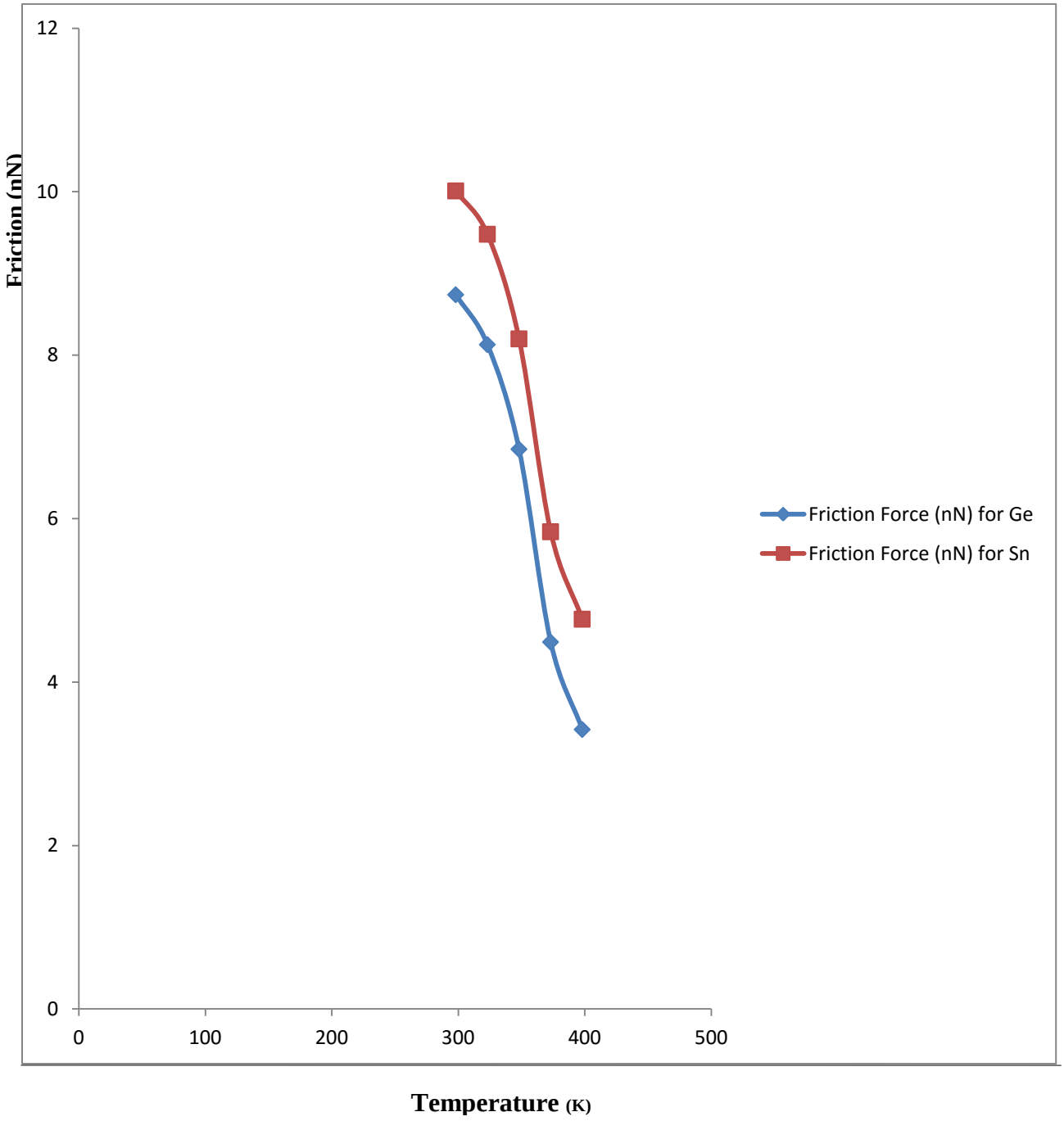

Fig. 4.2: Effects of temperature on nanotribology of Ge and Sn

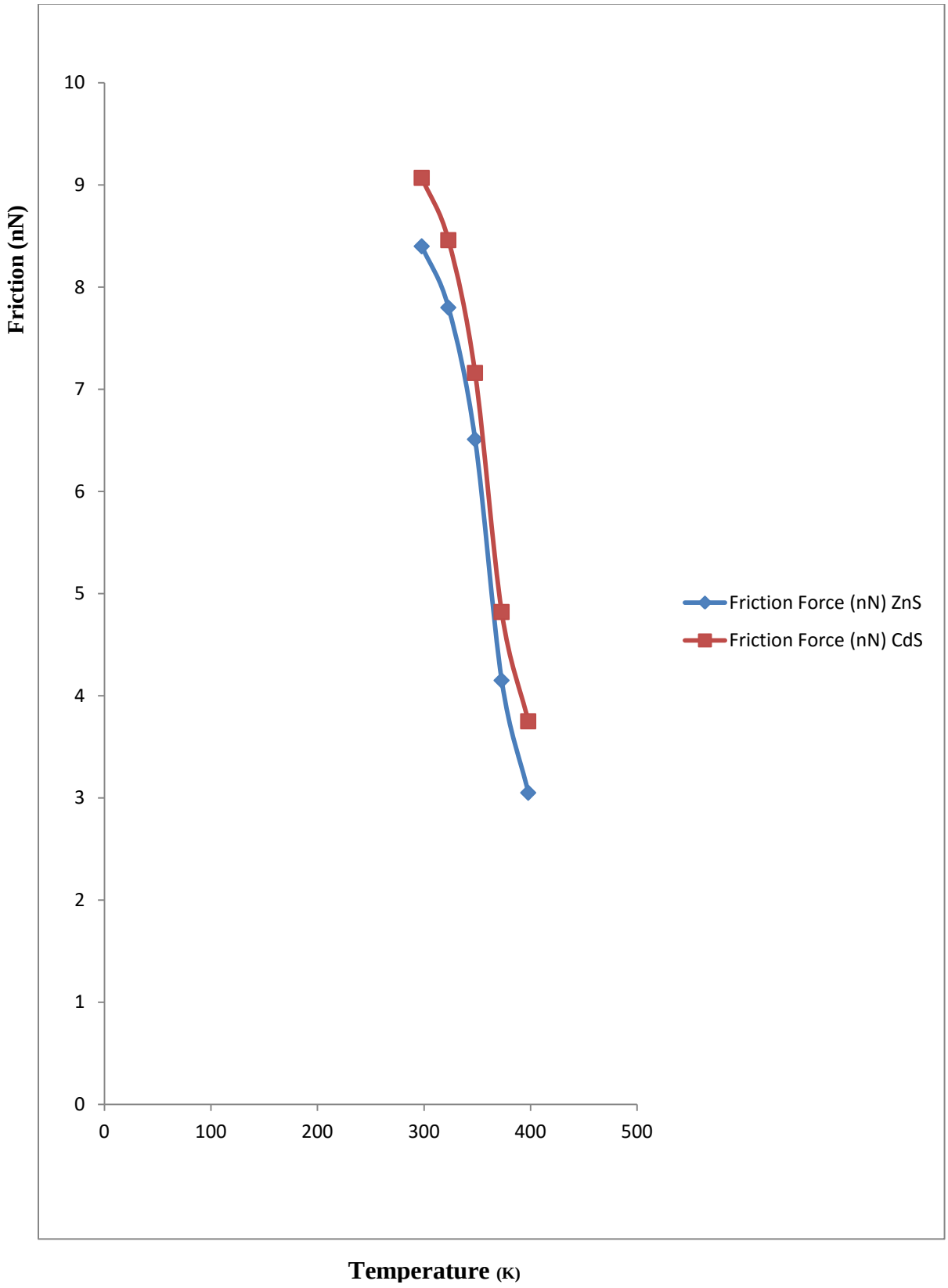

Fig. 4.3: Effects of temperature on nanotribology ZnS and CdS

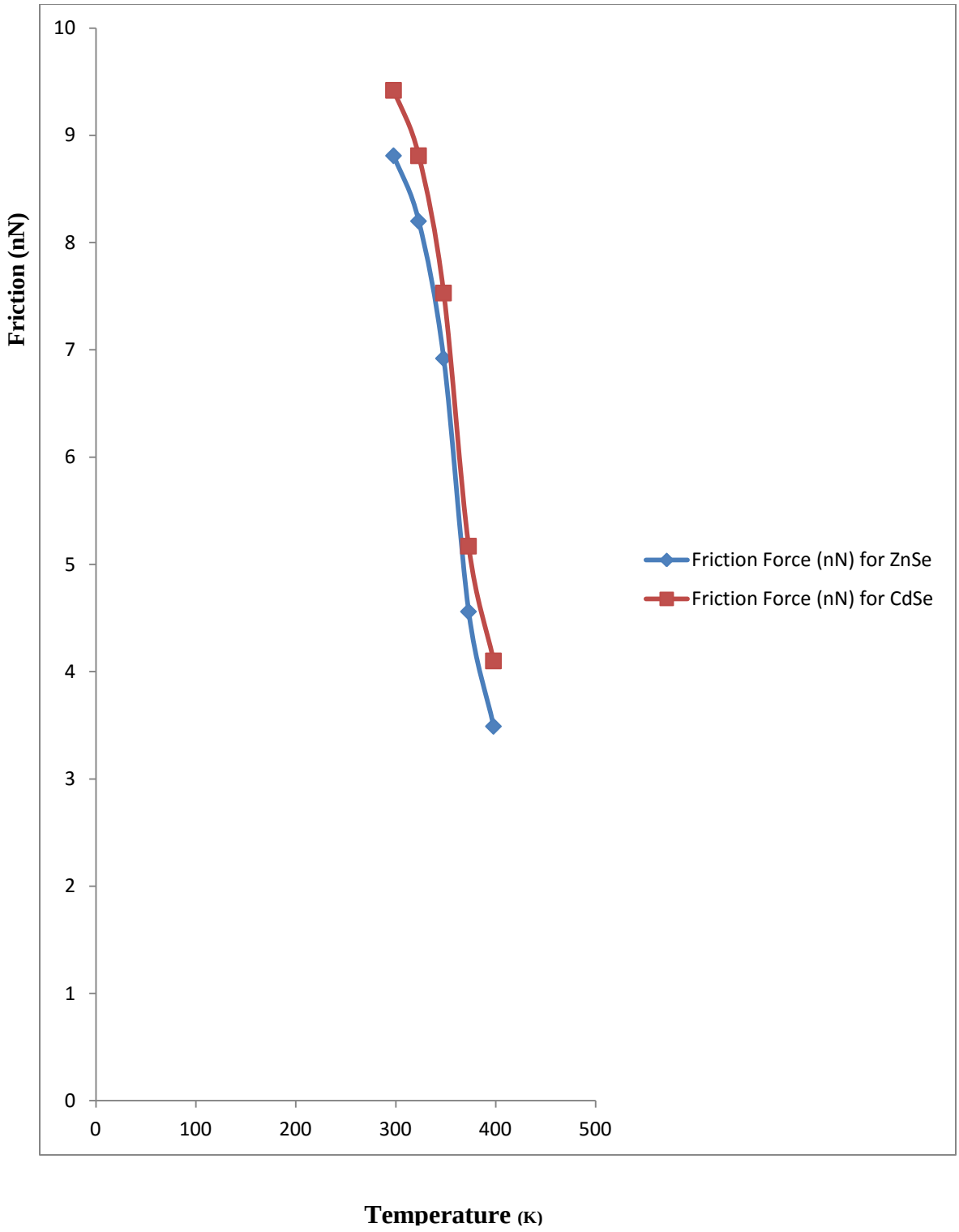

Fig. 4.4:Effects of temperature on nanotribology ZnSe and CdSe

The above results show that at nano-scale, friction decreases with increase in temperature. This agrees with the results obtained by (Robert, 2002; Bhushan, 2010; Gnecco *et al.*, 2010). The above results also agree with the results obtained by (Krylov and Frenken, 2014; Gnecco and Meyer, 2015) in which they found that nanotribology decreases with increase in temperature. The results also show that ZnS has the best tribological properties at various temperatures among the elements studied followed by silicon, germanium, zinc selenide, cadmium sulphide, cadmium selenide and tin. Tin, cadmium selenide and cadmium sulphide exhibit high values of friction at low temperatures. However, as the temperature increases, friction reduces to low values in each case.

From the graphs, it can be observed that nanotribological properties of elements become better as we move upwards in group IV elements in the periodic table. This may be due to less number of electrons present in the elements as we move upwards in the group. Also, as we move upwards according to periods, nanotribological properties of materials improve. This is observed with cadmium in period V and zinc in period IV. Again, as we move upwards in group VI, nanotribological properties improve. This is observed with selenium and sulphur in group VI. These observations further support the earlier conclusion that with less number of electrons in a material, such a material will exhibit better tribological properties with regard to temperature variations.

4.3 RESULTS OBTAINED FOR THE SEVEN SEMICONDUCTORS UNDER STUDY USING LOW AND HIGH VELOCITY MODELS

These models were used to study the effects of velocity on nanotribology of the seven semiconductors under study Si, Ge, Sn, ZnS, CdS, ZnSe and CdSe. The results obtained for silicon, together with the experimental results (Gnecco *et al.*, 2010) as found in literature are presented in Figure 4.5.

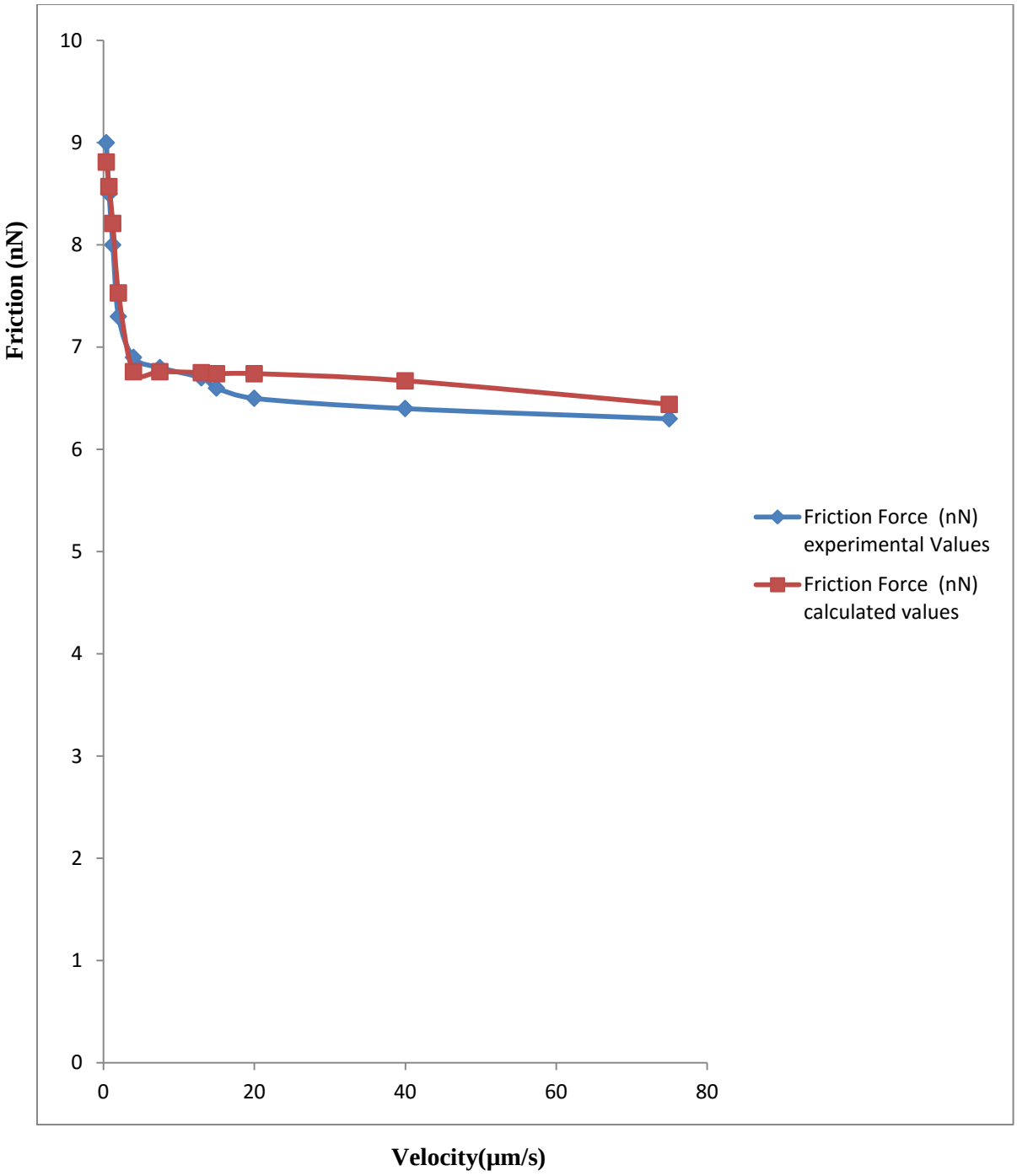

Fig 4.5: Theoritical effects of velocity on nanotribology of Si compared with experimental results of Si

Figure 4.5 shows that the results obtained for silicon using low and high velocity models compare favourably with experimental results. Hence this models can be used to predict experimental results properly. The models were also used to predict the values of frictional force for other six semiconductors – Ge, Sn, ZnS, CdS, ZnSe and CdSe.

The results obtained for these elements are presented according to the grouping: Ge and Sn, ZnS and CdS, ZnSe and CdSe in Figures 4.6, 4.7 and 4.8 respectively.

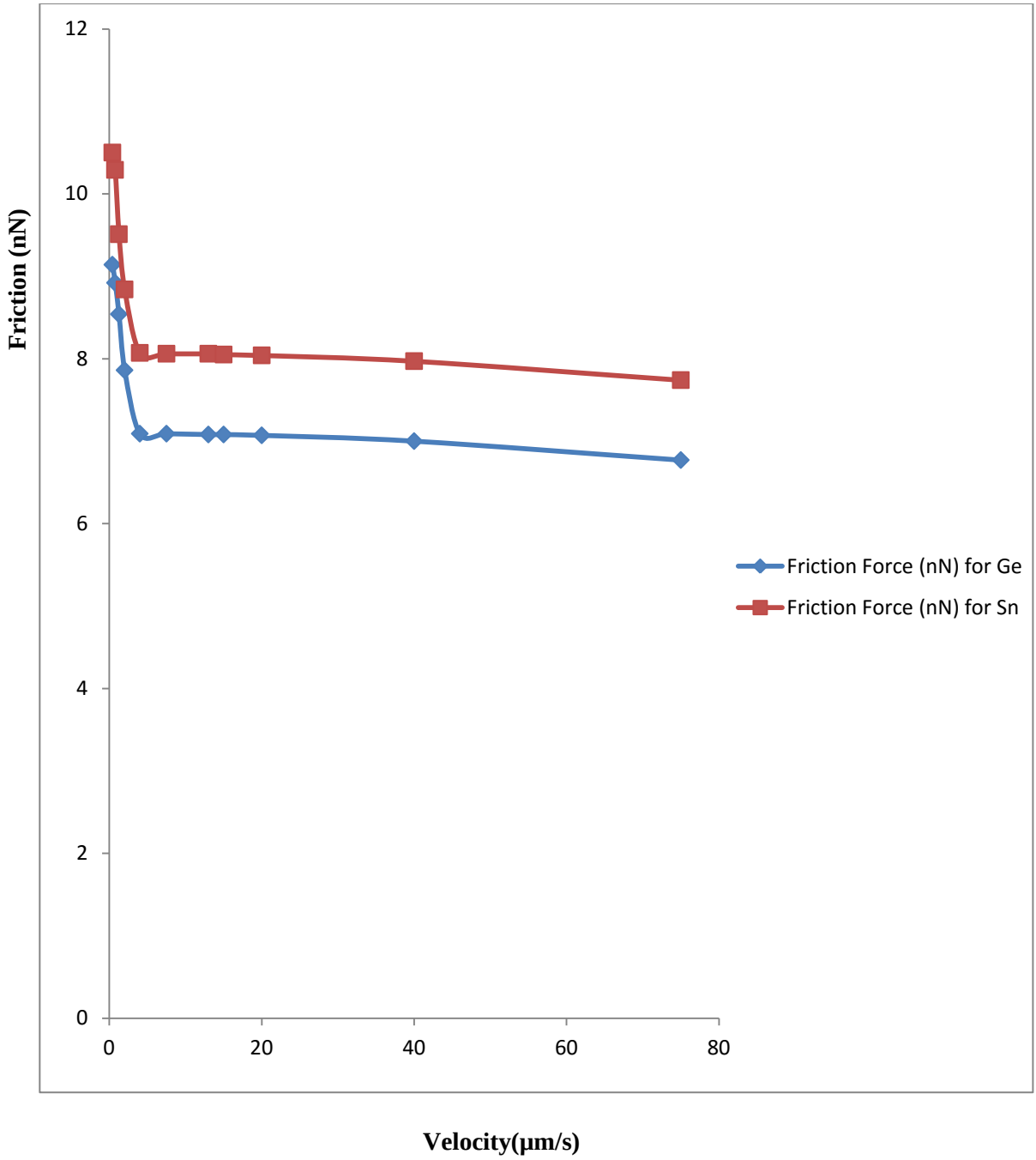

Fig. 4.6: Plots of the effects of velocity on nanotribology of Ge and Sn

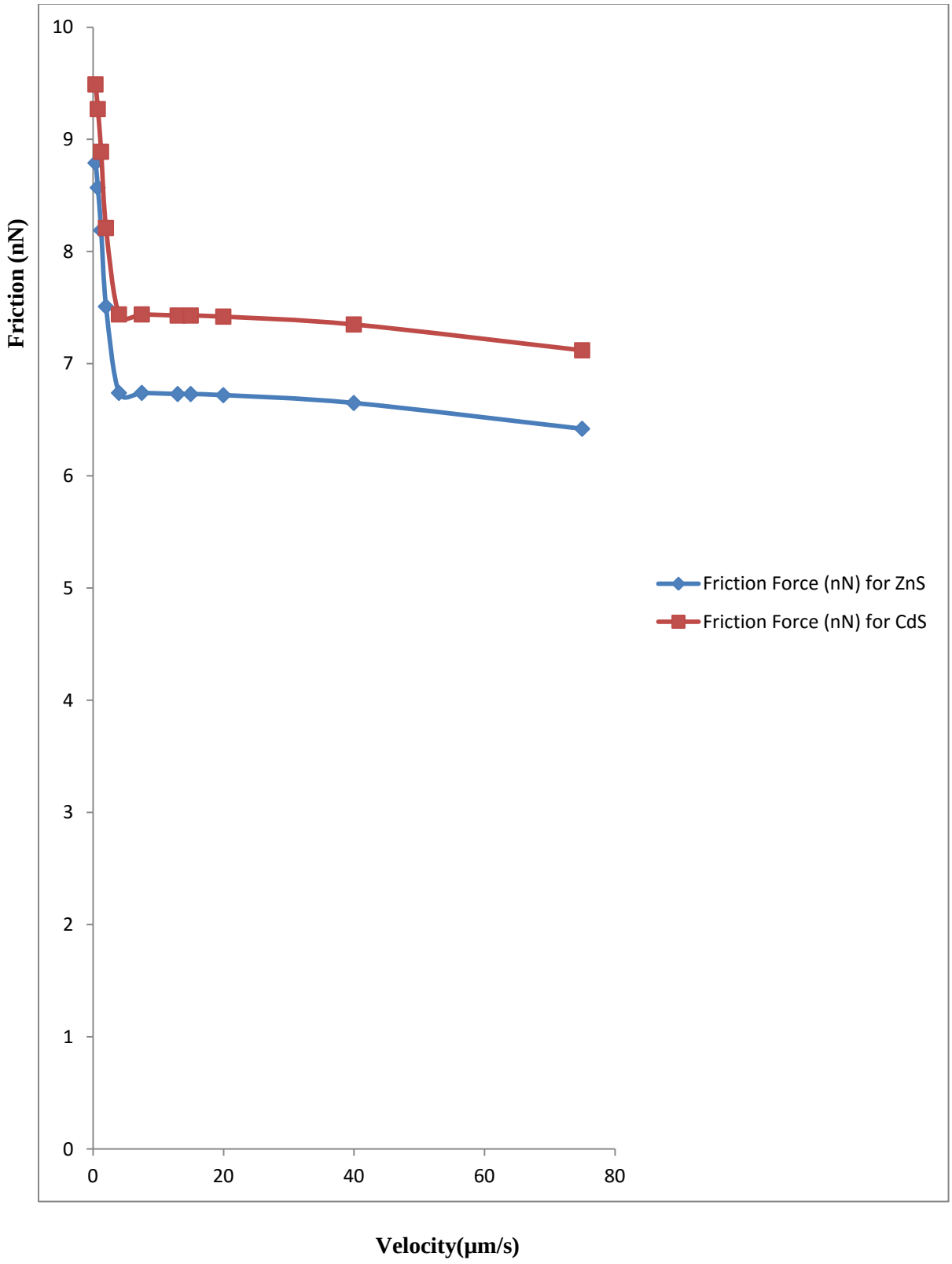

Fig. 4.7: Plots of the effects of velocity on nanotribology of ZnS and CdS

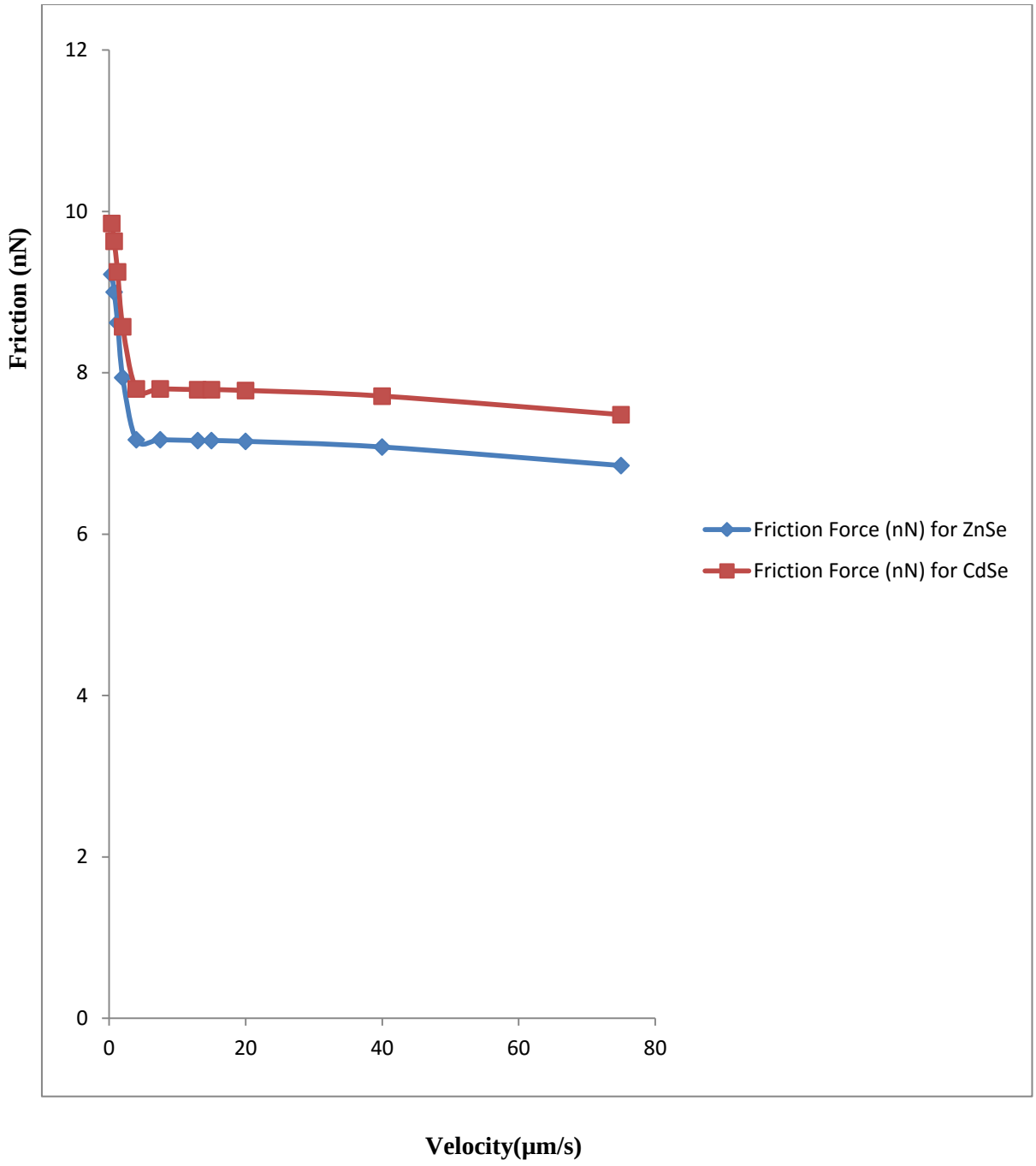

Fig. 4.8: Plots of the effects of velocity on nanotribology of ZnSe and CdSe

The above results show that friction decreases with increase in velocity at nano-scale. This agrees with the results obtained by (Liu and Bhushan, 2004; Bhushan, 2010). The above results also agree with the results obtained by (Sandoz-Rosando, 2013; Krylov and Frenken, 2014; Gnecco and Meyer, 2015) in which they found in their studies that nanotribology decreases with increase in sliding velocity. The results also show that ZnS exhibits better tribological properties due to its lower values of friction than other elements under study followed by Si, Ge and others. From the results, friction force decreases gradually as velocity increases and tends to be constant as velocity rises above 2.0 μm/s.

It can also be observed that as we move upwards in group IV elements, nanotribological properties become better with regard to velocity variation. This is also observed as we move upward in group VI elements. These observations may be due to less number of electrons present in these elements as we move upwards in the groups.

4.4: RESULTS OBTAINED USING NORMAL LOAD MODEL

This model was used to study the effects of normal load on the nanotribology of the seven semiconductors under study – Si, Ge, Sn, ZnS, CdS, ZnSe and CdSe. The results obtained for silicon together with the experimental results (Gnecco *et al.*, 2010) as found in literature are presented in Figure 4.9.

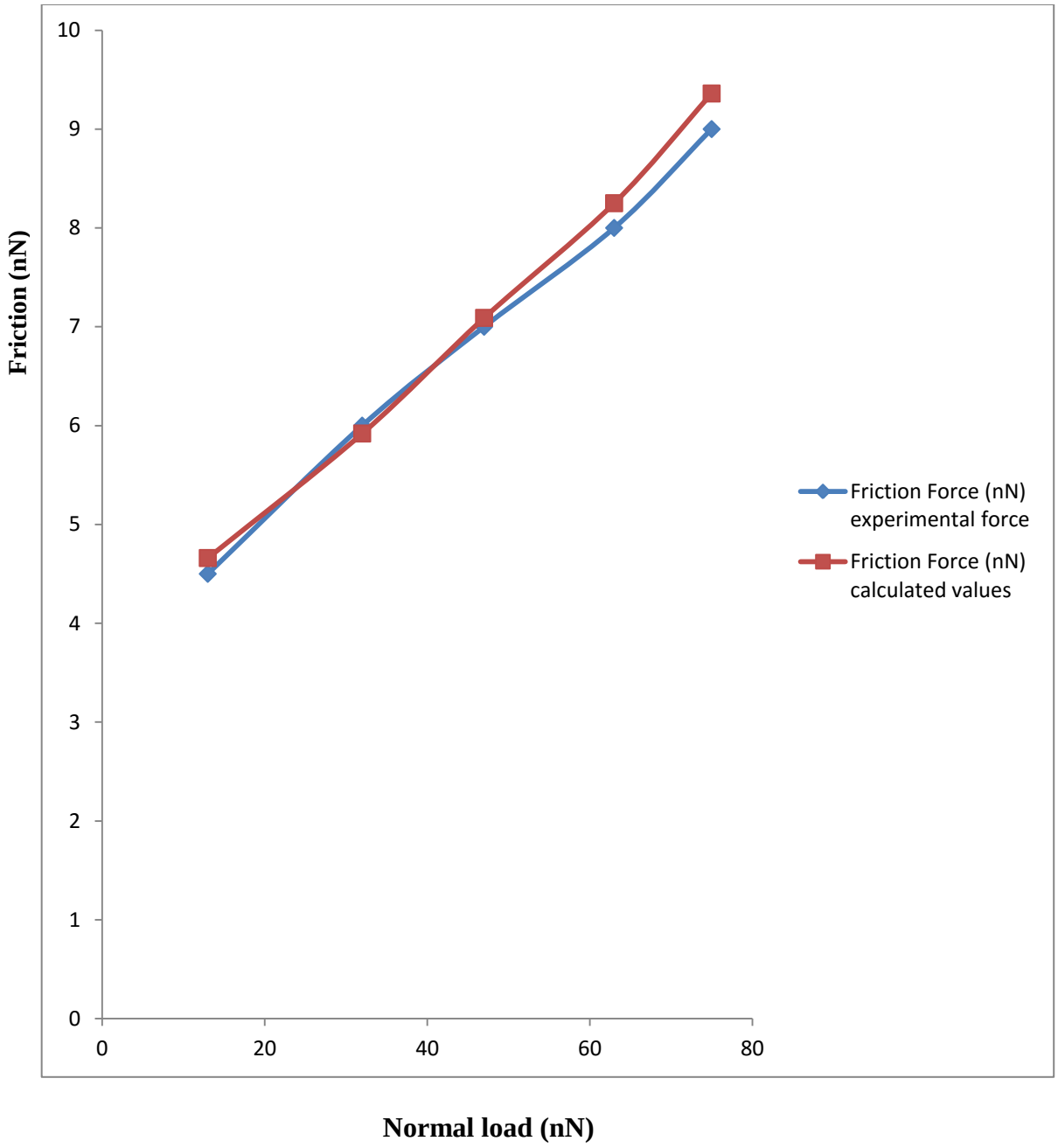

Fig. 4.9: Theoritical effects of normal load on nanotribology of Si together with experimental results of Si

The graphs show that the results obtained using normal load model compare favourably with experimental results found in literature. Hence the model can be used to predict experimental results properly. This model was also used for other six semiconductors under study – Ge, Sn, ZnS, CdS, ZnSe, and CdSe. The results obtained are presented according to the grouping Ge and Sn,
ZnS and CdS, ZnSe and CdSe in Figures 4.10, 4.11 and 4.12 respectively.

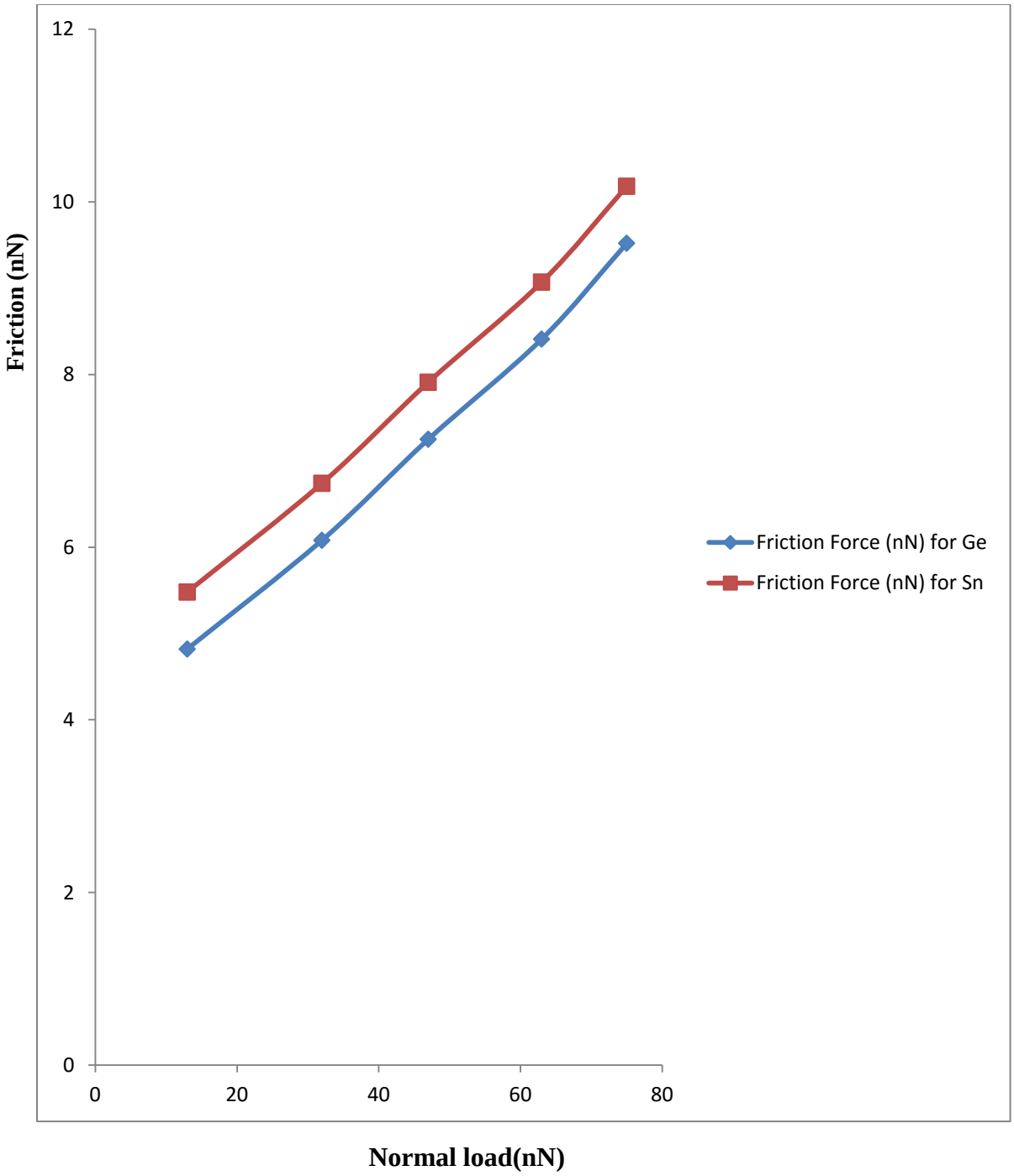

Fig. 4.10:Plots of the effects of normal load on nanotribology of Ge and Sn

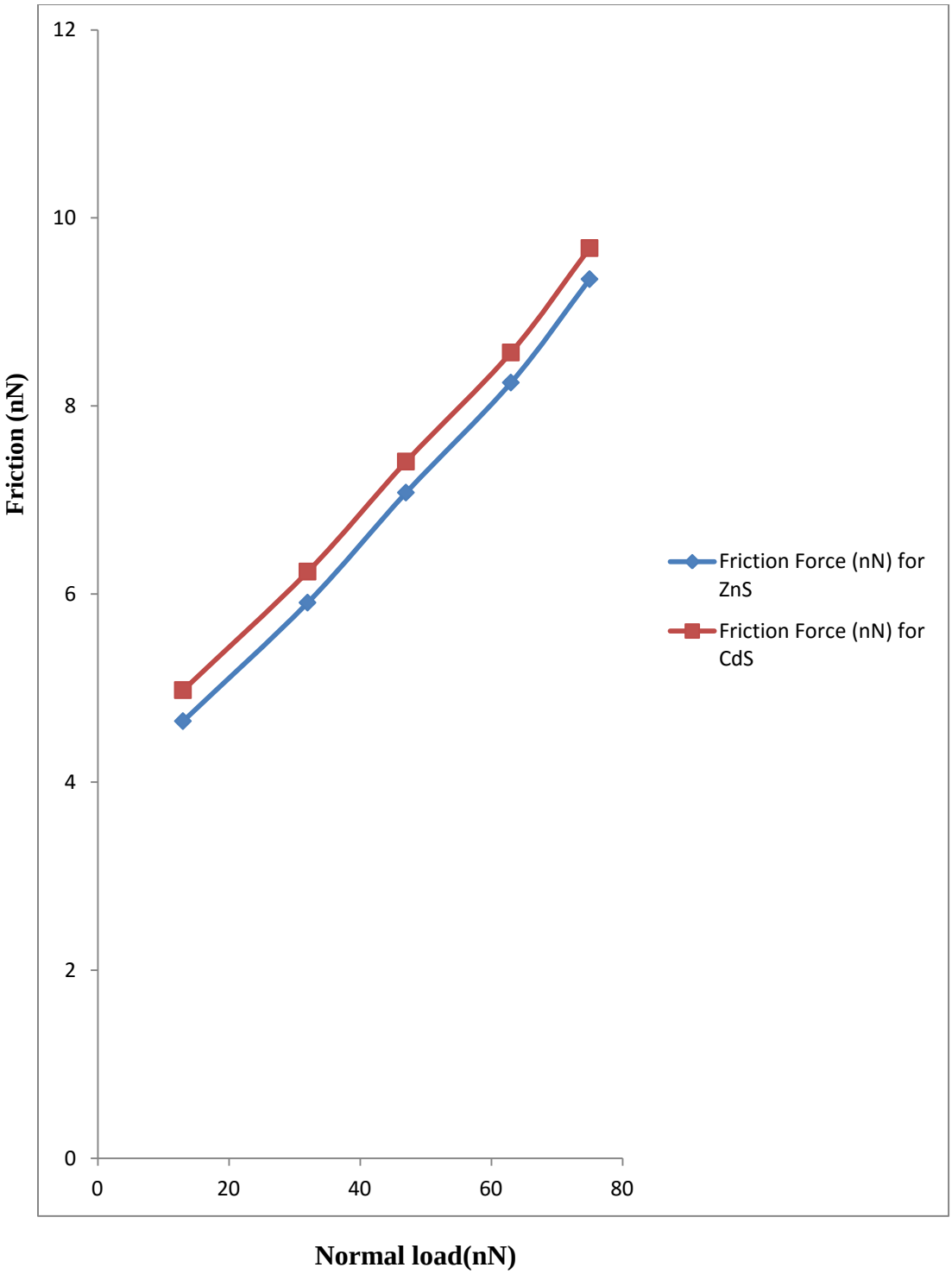

Fig. 4.11: Plots of the effects of normal load on nanotribology of ZnS and CdS

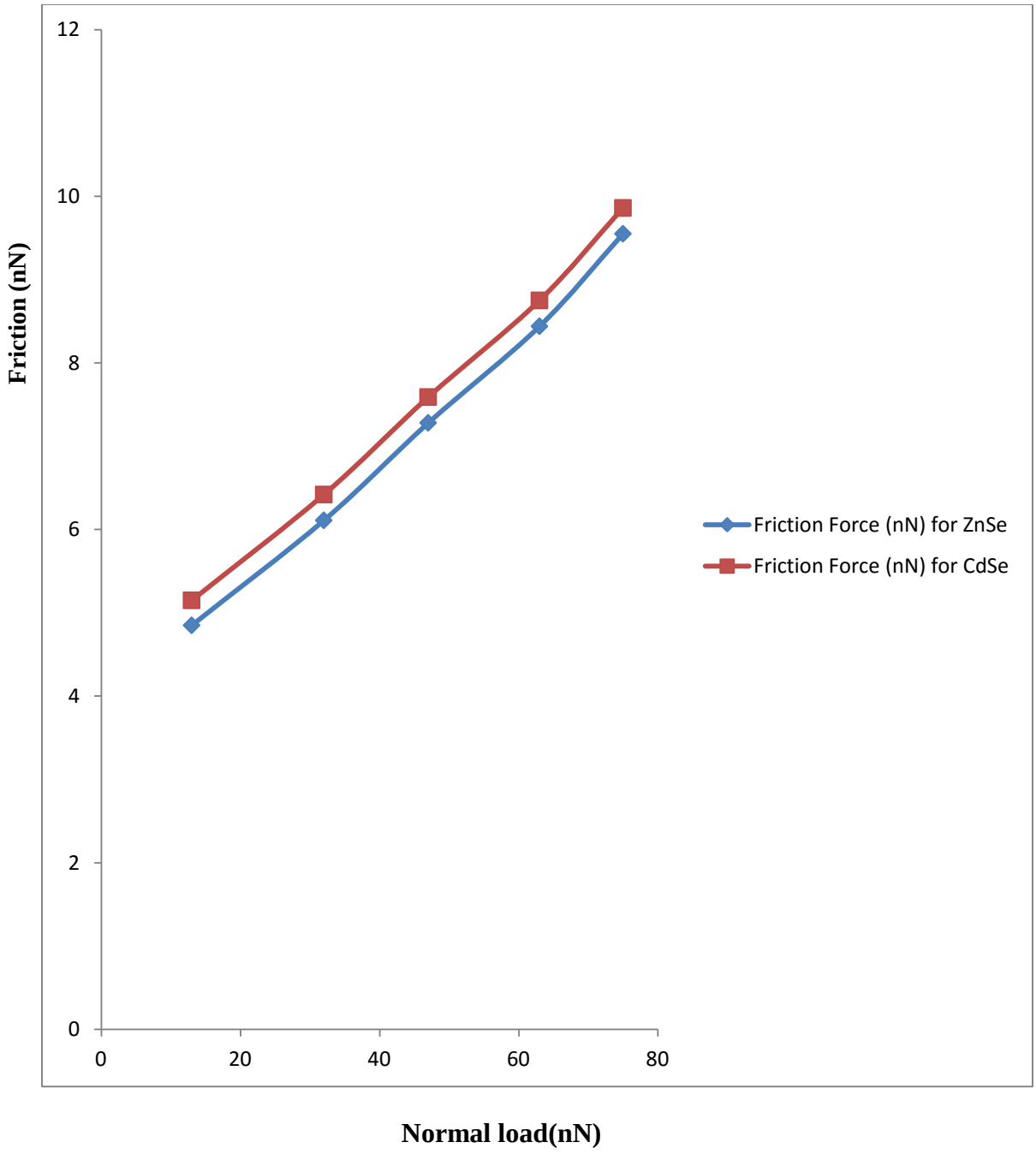

Fig. 4.12: Plots of the effects of normal load on nanotribology of ZnSe and CdSe.

From the above results, at nano-scale, friction increases with increase in normal load. This agrees with the results obtained by (Gnecco *et al.*, 2010; Carpick and Salmeron, 1997; Miser and Robbins, 2000; Liang *et al*., 2003). The above results also agree with the results obtained by (Nuruzzaman and Chowdhury, 2012; Sandoz-Rosado, 2013; Krylov and Frenken, 2014; Gnecco and Meyer, 2015) in which they found that nanotribology of materials increases with increase in normal load. The results also indicate that ZnS exhibits better tribological properties than other semiconductors under study, followed by Si.

At a maximum load of 75nN, the nano-friction existing in ZnS is 9.35nN while that of Si at the same normal load of 75nN is 9.36nN. Tin exhibits the highest nano-friction of 10.18nN at a normal load of 75.0nN among the elements studied. Since ZnS exhibits lower frictional forces at higher loads, it is recommended in applications where the normal load is likely to be high followed by silicon.

It can also be observed that as we go upwards in group IV elements in the periodic table, nanotribological properties of these elements improves with regard to normal load variations. This again may be due to less number of electrons present in these elements as we move upwards in the group. Also, as we move upwards in group VI elements of the periodic table, binary compounds formed from these elements exhibit better tribological properties with regard to normal

load variation. This is observed with ZnSe and ZnS with nanotribology of 9.55nN and 9.35 nN respectively at a normal load of 75.0nN. This observation also holds for CdSe and CdS with nano-friction values of 9.86nN and 9.68nN respectively at the same normal load of 75.0nN. These observations suggest that zinc oxide may exhibit exceptionally good nanotribological properties with regard to temperature, velocity and normal load variations. Tables containing the calculated and experimental values for all the semiconductors studied from which all the graphs were ploted are presented in appendix A. List of publications from the work are shown in appendix B.

CHAPTER FIVE

SUMMARY, CONCLUSION AND SUGGESTIONS FOR FURTHER WORK.

5.1 Summary.

In this work six new models were developed and used to study nanotribology of semiconductors. Jump energy quantum models were used to obtain values ΔE of which is the energy that prevents the tips jump in experiment with atomic force microscope or in friction force microscope. The results obtained are in good agreement with the results obtained using Tomlinson model. The results obtained show that with bond energy gap E_g, ΔE can be calculated for any semiconductor. The results also show that zinc sulphide has the highest value of ΔE among the seven semiconductors studied.

Temperature model which was used to study temperature dependence of nanotribology of semiconductors produced results which compare favourably with experimental results (Gnecco *et al*., 2010) for silicon available in literature. The results obtained show that this model can be used to predict experimental results.

The results also show that nanotribology decreases with increase in temperature. Since zinc sulphide has lower nano-friction at different temperatures, it possesses better tribological properties at various temperatures than other materials studied.

Low and high velocity models were used to study velocity dependence of nanotribology. The results obtained show that friction at nano-level decreases with increase in velocity. At velocities above 2.0μm/s, friction remains nearly constant. Again zinc sulphide showed better tribological properties when compared to other materials studied.

With normal load model, normal load dependence of nanotribology was studied. The results obtained compare favourably with experimental results for silicon found in literature. The results show that friction at nano-level increases with increase in external load. In this case, zinc sulphide also takes the lead in materials recommendation followed by silicon.

5.2: **CONCLUSION**

The six models developed in this research have been successfully applied in the study of nanotribology of some semiconductor surfaces. Our models predict results for Si that are in reasonable agreement with experimental data of Si. There are no experimental results for germanium tin, zinc sulphide, cadmium sulphide, zinc selenide, and cadmium selenide. Hence, we are predicting results for these

semiconductors for the first time using our models. Bringing friction to a halt remains a challenging problem to nanotribologists and technologists. The increase in surface-to-volume ratio that occurs when devices are scaled down in size make friction increasingly problematic in miniature instruments like micro and nano-electromechanical systems. Devices that work reliably usually have designs that avoid sliding contacts. Systems with moving components that come into contact with each other on the other hand suffer enormous problems due to stiction, friction and wear. Lubrication is not an option because the lubricant would be too viscous on the nanoscale and moreover, the adhesion forces introduced by liquids are strong enough to damage tiny devices. An effective way of checking this problem is by making appropriate choice of chemical composition, crystal structure and surface roughness (Frenken,2006).

Lubrication at nanoscale requires lubricants molecules which are non volatile, oxidation and temperature resistant, good adhesion, cohesion and self repairing or self regenerating. This condition require the application of organic film, if such organic film can stay intact under the application of forces and repair by itself. From the results of this work, the following can be inferred:

If micro and nano-electro- mechanical systems are designed to operate normally at fairly high temperatures, their efficiency will surely increase due to decrease in nanotribology.

If nano and microelectromechanical system can be designed to operate normally at high velocities, nano-friction may not pose much problem.

However, for low speed systems, materials with high value of ΔE such as zinc sulphide and silicon are recommended.

5.3 SUGGESTIONS FOR FURTHER WORK.

For further research in nanotribology of semiconductors, the following areas are suggested:

- Development of functional models to study the effects of wear, rest time, relative humidity, tip radius and number of cycles on nanotribology of semiconductor surfaces.
- Thin film development and characterization of nanotribological properties of germanium, tin, zinc sulphide, cadmium sulphide, zinc selenide, cadmium selenide and gallium arsenide.

References

Anczykowski, B. (2004). Dynamic force microscopy, Handbook of nanotechnology, ed. Bhushan, B., 1st edition, Berlin Heidelberg: Springer-Verlag.

Animalu, A.O.E. (1977). Intermediate quantum theory of crystalline solids, New Jersey: Prentice Hall Inc.

Anna, G.D., Benoit, W. and Vinokur, V.M. (1997). Internal friction and dislocation collective pinning in disordered quenched solid solutions, J. App. Phys 82, 5983-5990.

Batteas, J.D. (2004). Scanning probe studies of nanoscale adhesion between solids in the presence of liquid and monolayer films, Handbook of nanotechnology, ed. Bhushan, B., 1st edition, Berlin Heidelberg: Sringer-Verlag.

Bhushan, B. and Liu, H. (2004). Self-assembled monolayers for controlling adhesion, friction and wear, Handbook of nanotechnology, ed. Bhushan, B., 1st edition, Berlin Heidelberg: Sringer-Verlag.

Bhushan, B. and Marti, O. (2010). Scanning probe microscopy - principle of operation, instrumentation and probes, Handbook of nanotechnology, ed. Bushan B., 3rd edition, Berlin Heidelberg: Sringer-Verlag.

Bhushan, B. (2010). Nanotribology, nanomechanics and materials characterization, Handbook of nanotechnology, ed. Bhushan B, 3rd edition, Berlin Heidelberg: Sringer-Verlag.

Bhushan, B. and La Torre, C. (2010). Structural, nanomechanical and nanotribological characterization of human hair using atomic force microscopy and nanoindentation, Handbook of nanotechnology, ed. Bhushan B., 3rd edition, Berlin Heidelberg: Sringer-Verlag.

Braun, J., Fuhrmann, D., Siber, A., Gumhalter, B. and Woll, Ch. (1998). Observation of a zone- center GaP in the longitudinal mode of an adsorbate overlayer: Xe Cu (111), Phys. Rev. Lett. 80, 125 - 128.

Bruch, L.W. and Hansen, F.Y. (1997). Mode damping in a commensurate monolayer solid, Phys. Rev. B 55, 1782 - 1792.

Carpick, R.W. and Salmeron, M. (1997). Fundamental investigations of tribology with atomic force microscope, Chem. Rev. 97, 1163 - 1194.

Chandross, M., Webb III, E.B., Stevens, M.J., Grest, G.S. and Garofalini, S.H.(2004). Systematic study of the effect of disorder on nanotribology of self assembled monolayers, Phys. Rev. Lett. 93, 166103 - 1661011.

Chang, S.C. and Chang, T. (2007). Grain size effect on nanomechanical properties and deformation behavior of copper under nanoindentation test, J. Appl. Phys. 101, 033507- 033512.

Cieplak, M., Smith, E.D. and Robbins, M.O. (1994). Molecular origins of friction: the force on adsorbed layers, Science 265, 1209 - 1212.

Daly, C. and Krim, J. (1996). Sliding friction of solid xenon monlayers and bilayers on Ag (111), Phys. Rev. lett. 76, 803 - 806.

Dayo, A., Alnasrallah, W. and Krim, J. (1998). Superconductivity-dependent sliding friction, Phys. Rev. Lett. 80, 1690 - 1693

Dayo, A. and Krim, J. (1998). Atomic- scale friction in Xe/Ag and N_2/Pb, International J. of thermophysics, 19, 827 - 834.

De Boer, M. P., Corwin, A. D., Del Rio, F. W. and Ashurst, W. R. (2010). Friction and wear in micro-and nanomachines, Handbook of nanotechnology, ed. Bhushan B., 3rd edition, Berlin Heidelberg: Sringer-Verlag.

Dinelli, F., Leggett, G.J. and Alexander, M.R. (2002). Nanowear in scanning force microscope: information on deposits formed in and downstream of a hexane plasma, J. Appl. Phys. 91, 3841 - 3846.

Doremus, R.H. (2002). Viscosity of silica, J. Appl. Phys. 92, 7619 - 7629.

Eldrid, S., Arne, T.S., Jorgen, A. and Geir, A. (2007). Local viscoscity measurements using oscillating magnetic holes, J. Appl. Phys. 101, 054910 - 054915.

Fraxedas, J., Garcia-Manyes, S., Gorostiza, P. and Sanz, F. (2002). Nanoindentation: towards the sensing of atomic interactions, PNAS, 99, 85228 - 85232.

Frenken, J. (2006). Nanotribology: bringing friction to a halt, News and Views 1, 20 - 21.

Fujita, K., Watanabe, H. and Ichikawa, M. (1998). Scanning tunneling microscopy study on the surface and interface of Si (111) SiO_2 structures., J. Appl. Phys., 83, 3638-3642.

Fujisawa, S., Kishi, E., Sugawara, Y. and Morita, S. (1994). Fluctuations in two-dimensional stick- slip phenomenon observed with two-dimensional friction force microscope, J.App. Phys, 33, 3752 - 3755

Gary, L.M. and Donald, A.T. (2004). Inorganic Chemistry, New Jersey: Pearson Prentice Hall.

Germann, G. J., Cohen, S. R., Neubauer, G., McCelland, G. M., Seki, H. and Coulman, D. (1993). Atomic scale friction of a diamond tip on diamond (100) and (111) surfaces, J. App. Phy., 73, 163 - 166.

Gnecco, E., Bennewitz, R., Pfeiffer, O., Socoliuc, A. and Meyer, E. (2010). Friction and wear on the atomic scale, Handbook of nanotechnology, Ed. Bhushan B. 3rd edition, Berlin Heidelberg: Sringer-Verlag.

Gnecco, E. and Meyer, E. (2015). Experimental results in nanotribology, Elements of Friction theory and Nanotribology, ed. Gnecco, E and Meyer, E., Cambridge University Press. P.196.

Gyalog, T. and Thomas, H. (1997). Atomic friction. Z. Phys. B., 104, 669 - 674.

Hafner, J.H. (2004). Probes in scanning microscopies, Handbook of nanotechnology, ed. Bhushan B. 1st edition, Berlin Heidelberg: Sringer-Verlag.

Hirano, M., Shinjo, K., Kaneko, R. and Murata, Y. (1991), Anisotropy of frictional forces in muscovite mica, Phys Rev. Lett. 67, 2642 - 2645.

Holscher, H., Ebeling, D., and Schwarz, U. D. (2008). Friction at atomic scale surface steps: experiment and theory, arxiv:0810.0165v1 (con-mat.other).

Honma, M. and Nose, T. (2007). Friction as the fundamental factor controlling the pretilt angle of homeotropic liquid crystal cells: a microrubbing investigation, J. Appl. Phys. 101, 104903 - 104908.

Ibach, H. and Luth, H. (2004). Solid-State Physics: An introduction to principles of materials science, (India): Springer Private Limited.

Isrealachvili, J.N. and Ruths, M. (2010). Surface forces and nanorheology of molecularly thin films, Handbook of nanotechnology, ed., Bhushan B. 3rd edition, Berlin Heidelberg: Sringer-Verlag.

Jang, I., Burris, D. L., Dickrell, P.L., Barry, P.R., Santos, C., Perry, S.S., Phillpot, S.R., Sinnotc, S.B. and Sawyer, W.G. (2007). Sliding effect on the tribological properties of ploytetrafluoroethylene, J.Appl. Phys. 102, 123509 - 123513.

Joly- Pottuz, L., Matta, C., de Barros Bouchet, M.I., Vacher, B., Martin, J.M. and Sagawa, T. (2007). Superlow friction of ta-C lubricated by glycerol: an electron energy loss spectroscopy study, J. Appl. Phy 102, 064912 - 064918.

Krim, J., Solina, D.H. and Chiarello, R. (1991). Nanotribology of a Kr monolayer: a quartz-crystal microbalance study of atomic scale friction, Phys. Rev. lett., 66, 181-184.

Krim, J. (2012). Friction and energy dissipation mechanisms in adsorbed molecules and molecularly thin films, Advances in Physics, 61, 155 – 323.

Krylov, S.Y. and Frenken, J.W.M. (2014). The physics of atomic-scale friction: basic considerations and open questions, Phys. Status Solidi B 251, 711 -736

Kutzelnigg, W. (1996). Friedrich Hund and Chemistry, Angewandte Chemie International, 35, 573 - 586.

La Rosa, A., Li, N. and Asante, K. (2005). The shear-force/ ultrasonic near-field microscope : a nanometrology tool for surface science and technology. SPIE, SA III, 31 - 36.

Lennard-Jones, J. (1929). The electronic structure of some diatomic molecules. Transactions of the Faraday Society, 25, 668 - 686.

Lee, K.L. and Kui, H.W. (1994). Scaling of viscosities of glass forming alloys, J. Appl. Phys. 76, 2694 - 2696.

Liang, Q., Tsui, O.K.C., Xu, Y., Li H., and Xiao, X. (2003). Effect of C_{60} molecular rotation on nanotriboology Phy Rev. Letters 90, 146102-1 - 146102-4.

Liu, H. and Bhushan, B. (2004). Nanoscale boundry lubrication studies, Handbook of nanotechnology, ed. Bhushan B., 1st edition, Berlin Heidelberg: Sringer-Verlag.

Mann, A.B. (2004). Nanomechanical properties of solid surfaces and thin films. Handbook of nanotechnology, ed. Bhushan B., 1st edition, Berlin Heidelberg: Sringer-Verlag .

Mate, C.M., McClelland, G.M., Erlandson, R. and Chiang, S. (1987). Atomic scale friction of a tungsten tip on a graphite surface, Phys. Rev. Lett. 59, 1942 - 1945.

Martin, H.M. (2004). Atomistic computer simulations of nanotribology. Handbook of nanotechnology, ed. Bhushan B., 1st edition, Berlin Heidelberg: Sringer-Verlag .

,

McGguiggan, P.M. and Isrealachvili, J.N. (1990). Adhession and short-range forces between surfaces. Part II: effects of surface lattice mismatch. J. Mater. Res. 5, 2232 - 2243.

Mulliken, R.S. (1967). Nobel lecture, Science 157, 13 - 24.

Muser, M.H and Robbins, M.O. (2000). Friction between flat crystalline surfaces, Phys. Rev. B61, 2335 - 2342

Novotny, T. and Velicky, B. (1999), Electronic sliding friction of atoms physisorbed at superconductor surface, Phys. Rev. Lett. 83, 4112 - 4115.

Nuruzzaman, D.M. and Chowdhury, M. A. (2012). Effects of normal load and sliding velocity on friction coefficient of aluminum sliding against different pin materials, American Journal of Materials Science, 2, 26 - 31

Persson, B.N.J. (1991). Surface resistivity and vibrational damping in adsorbed layers, Phys. Rev. B44, 3277 - 3296.

Renner, R.L., Rutledge, J.E. and Taborek, P. (1999). Quartz microbalance studies of superconductivity- dependent sliding friction, Phys. Rev. Lett. 83, 1261 - 1261.

Robert, H.D. (2002). Viscosity of silica, J. App. Phys. 92, 7619 - 7629

Ruffel, S., Bradby, J.E., Fujisawa, N. and Williams, J.S. (2007). Identification of nanindentation-induced phase changes in silicon by insitu electrical characterization, J. Appl. Phys. 101, 083531 - 083538.

Sacco, J.E. and Sokoloff, J.B. (1978). Free sliding in lattices with two incommensurate periodicities, Phys. Rev. B18, 6549 - 6559.

Sandoz-Rosado, E.J. (2013). The tribological behaviour of graphene and its role as a protective coating, Ph.D thesis, Graduate School of Arts and Science, Columbia University P. 5 - 16.

Scharf, T.W., Ott, R.D., Yang, D. and Barnard, J.A. (1998). Structural and tribological characterisation of protective amorphous diamond-like carbon and amorphous CN_x overcoats for next generation hard disk, J. Appl. Phys. 85, 3142 - 3154.

Shinjo, K and Hirano, M. (1993). Dynamics of friction: superlubric state, Surf Sci. 283, 473 - 478.

Smith, E.D. Rubbins, M.O. and Cieplak, M. (1996). Friction on adsorbed monolayers, Phys. Rev. B 54, 8252 - 8260.

Sokoloff, J.B., Sacco, J.E. and Weiz, J. F. (1978). Undamped lattice vibrations in systems with two incommensurate periodicities, Phys. Rev. Lett 41, 1561 - 1564.

Sundararajan, S. and Bhushan, B. (2000). Topography-induced contributions to friction forces measured using an atomic force/ friction force microscope, J. Appl. Phys. 88, 4825 - 4831.

Sundararajan, S. and Bhushan, B. (2001). Static friction and surface roughness studies of surface micromachined electrostatic micromotors using an atomic force/friction force microscope, J. Vac. Sc. Technology A19, 1777 - 1785.

Sundip, B., Michel, W. B., Adrian, D. W. and Moustakas, T. D. (2007). Spherical nanoindentation and deformation mechanisms in freestanding GaN films, J. Appl. Phys. 101, 083522 - 083527.

Suman, C., Jamal, D. and Shubhasish, C., (2007). A generalized model for probing frictional characteristics of pressure-driven liquid microflows. J. Appl. Phys., 102, 104907 - 104911.

Terada, Y., Harada, M., Ikehara, T., and Nishi, T. (2000). Nanotribology of polymer blends, J. Appl. Phys. 87, 2803 - 2807.

Toennies, J.P. (1993). The interaction of atoms with semiconductor surfaces : the case of Sb on GaAs(110). J. Phys. Condens .Matt. 5, 25 - 40.

Tomassone, M.S., Sokoloff, J.B., Widom, A. and Krim, J. (1997). Dominance of phonon friction for a xenon film on a silver (III) surface, Phys Rev. Lett. 79, 4798 - 4801

Tomlinson, G.A. (1929). A molecular theory of friction, J. of Sci. 7, 4798 - 4801.

Williams, S., Leslie, I., Isaac, G., Jin, Z., Ingham, E. and Fisher, J. (2008). Tribology and wear of metal-on metal hip prostheses: Influence of cup angle and head position, Journal of Bone and Joint Surgery, 90, 111 - 117.

APPENDIX A: TABLES

Table 2: Results obtained for silicon using temperature model together with experimental results of Si (Gnecco *et al*., 2010) found in literature.

Temperature (K)	Friction force (nN) calculated values	Friction force (nN) experimental values
298	8.42	8.50
323	7.81	8.00
348	6.51	6.50
373	4.17	3.50
398	3.07	3.00

Table 3: Results obtained for Ge using temperature model.

Temperature (K)	Friction Force (nN)
298	8.74
323	8.13
348	6.85
373	4.49
398	3.42

Table 4: Results obtained for Sn using temperature model.

Temperature (K)	Friction Force (nN)
298	10.01
323	9.48
348	8.20
373	5.84
398	4.77

Table 5: Results obtained for ZnS using temperature model.

Temperature (K)	Friction Force (nN)
298	8.40
323	7.80
348	6.51
373	4.15
398	3.05

Table 6: Results obtained for CdS using temperature model

Temperature (K)	Friction Force (nN)
298	9.07
323	8.46
348	7.16
373	4.82
398	3.75

Table 7: Results obtained for ZnSe using temperature model

Temperature (K)	Friction Force (nN)
298	8.81
323	8.20
348	6.92
373	4.56
398	3.49

Table 8: Results obtained for CdSe using temperature model.

Temperature (K)	**Friction Force (nN)**
298	9.42
323	8.81
348	7.53
373	5.17
398	4.10

Table 9: Results obtained for Si using low and high velocity models together with experimental results of Si (Gnecco *et al*., 2010) found in literature.

Velocity (μm/s)	**Friction force (nN) Calculated values**	**Friction force (nN) experimental values**
0.40	8.81	9.00
0.75	8.57	8.50
1.25	8.21	8.00
2.00	7.53	7.30
4.00	6.76	6.90
7.50	6.76	6.80
13.00	6.75	6.70
15,00	6.74	6.60
20.00	6.74	6.50
40.00	6.67	6.40
75.00	6.44	6.30

Table 10: Results obtained for Ge using low and high velocity models

Velocity (μm/s)	**Friction force (nN)**
0.40	9.14
0.75	8.92
1.25	8.54
2.00	7.86
4.00	7.09
7.50	7.09
13.00	7.08
15,00	7.08
20.00	7.07
40.00	7.00
75.00	6.77

Table 11: Results obtained for Sn using low and high velocity models

Velocity (μm/s)	**Friction force (nN)**
0.40	10.5
0.75	10.29
1.25	9.51
2.00	8.84
4.00	8.07
7.50	8.06
13.00	8.06
15,00	8.05
20.00	8.04
40.00	7.97
75.00	7.74

Table 12: Results obtained for ZnS using low and high velocity models

Velocity (μm/s)	Friction force (nN)
0.40	8.79
0.75	8.57
1.25	8.19
2.00	7.51
4.00	6.74
7.50	6.74
13.00	6.73
15.00	6.73
20.00	6.72
40.00	6.65
75.00	6.42

Table 13: Results obtained for CdS using low and high velocity models

Velocity (µm/s)	**Friction force (nN)**
0.40	9.49
0.75	9.27
1.25	8.89
2.00	8.21
4.00	7.44
7.50	7.44
13.00	7.43
15,00	7.43
20.00s	3.42
40.00	7.35
75.00	7.12

Table 14: Results obtained for ZnSe using low and high velocity models

Velocity (μm/s)	Friction force (nN)
0.40	9.22
0.75	9.00
1.25	8.62
2.00	7.94
4.00	7.17
7.50	7.17
13.00	7.16
15,00	7.16
20.00	7.15
40.00	7.08
75.00	6.85

Table 15: Results obtained for CdSe using low and high velocity models

Velocity (μm/s)	Friction force (nN)
0.40	9.85
0.75	9.63
1.25	9.25
2.00	8.57
4.00	7.80
7.50	7.80
13.00	7.79
15,00	7.79
20.00	7.78
40.00	7.71
75.00	7.48

Table 16: Results obtained for silicon using normal load model together with experimental results of Si (Gnecco *et al*., 2010) available in literature

Normal load (nN)	**Friction force (nN)** **calculated values**	**Friction force (Nn)** **experimental values**
13.00	4.66	4.50
32.00	5.92	6.00
47.00	7.09	7.00
63.00	8.25	8.00
75.00	9.36	9.00

Table 17: results obtained for Ge using normal load model.

Normal load (nN)	**Friction force (nN)**
13.00	4.82
32.00	6.08
47.00	7.25
63.00	8.41
75.00	9.52

Table 18: Results obtained for Sn using normal load model.

Normal load (nN)	Friction force (nN)
13.00	5.48
32.00	6.74
47.00	7.91
63.00	9.07
75.00	10.18

Table 19: Results obtained for ZnS using normal load model.

Normal load (nN)	Friction force (nN)
13.00	4.65
32.00	5.91
47.00	7.08
63.00	8.25
75.00	9.35

Table 20: Results obtained for CdS using normal load model

Normal load (nN)	Friction force (nN)
13.00	4.98
32.00	6.24
47.00	7.41
63.00	8.57
75.00	9.68

Table 21: Results obtained for ZnSe using normal load model

Normal load (nN)	Friction force (nN)
13.00	4.85
32.00	6.11
47.00	7.28
63.00	8.44
75.00	9.55

Table 22: Results obtained for CdSe using normal load model.

Normal load (nN)	**Friction force (nN)**
13.00	5.15
32.00	6.42
47.00	7.59
63.00	8.75
75.00	9.86

APPENDIX B: LIST OF PUBLICATIONS FROM THE WORK

Olisakwe, S.I., Ekpunobi, A. J. and Ekwo, P. I. (2012). Effects of temperature on the nanotribology of zinc selenide (ZnSe) and cadmium selenide (CdSe), Chalcogenide Letters, 9, 307 – 313.

Olisakwe, S.I., Ekpunobi, A. J. and Ekwo, P. I. (2012). Effects of temperature on the nanotribology of ZnS and CdS, Journal of Science and Arts, 18, 51 – 56.

Olisakwe, S.I., Ekpunobi, A. J. and Ekwo, P. I. (2012). Effects of temperature on the nanotribology of silicon (Si), germanium (Ge) and tin (Sn), Advances in Environmental Biology, 6, 1489 – 1493.

Olisakwe, S.I., Ekpunobi, A. J. and Ekwo, P. I. (2014). Effects of velocity on nanotribology of silicon (Si), germanium (Ge) and tin (Sn), Asian Journal of Applied Sciences, 2, 711 – 716.

Olisakwe, S.I., Ekpunobi, A. J. and Ekwo, P. I. (2015). Effects of normal load on nanotribology of zinc sulphide (ZnS) and cadmium sulphide (CdS), British Journal of applied Science and Technology, 10, 1 -7.